Front. Phys. 12(5), 126402 (2017)
DOI 10.1007/s11467-016-0632-z

RESEARCH ARTICLE

Renormalization-group theory of first-order phase transition dynamics in field-driven scalar model

Fan Zhong

State Key Laboratory of Optoelectronic Materials and Technologies, School of Physics, Sun Yat-sen University, Guangzhou 510275, China
E-mail: stszf@mail.sysu.edu.cn
Received August 23, 2016; accepted October 8, 2016

Through a detailed study of the mean-field approximation, the Gaussian approximation, the perturbation expansion, and the field-theoretic renormalization-group analysis of a φ^3 theory, we show that the instability fixed points of the theory, together with their associated instability exponents, are quite probably relevant to the scaling and universality behavior exhibited by the first-order phase transitions in a field-driven scalar ϕ^4 model, below its critical temperature and near the instability points. Finite-time scaling and leading corrections to the scaling are considered. We also show that the instability exponents of the first-order phase transitions are equivalent to those of the Yang–Lee edge singularity, and employ the latter to improve our estimates of the former. The outcomes agree well with existing numerical results.

Keywords first-order phase transitions, renormalization group theory, ϕ^3 theory, scaling and universality, instability exponents, Yang–Lee edge singularity, finite-time scaling, corrections to scaling, scalar model, dynamics, hysteresis

PACS numbers 64.60.Bd, 64.60.ae, 05.70.Fh, 64.60.My

1 Introduction

Phase transitions are of great importance in almost all scientific fields. Traditionally, a phase transition is said to be nth order if the nth derivative of the chemical potentials of the two involved phases is discontinuous at the transition point, and all lower-order derivatives are continuous [1]. However, transitions of orders higher than one often exhibit singularities in their transition points. At present, only first-order or discontinuous phase transitions (FOPTs) are usually distinguished from continuous transitions that include all other orders [2]. The first recorded continuous phase transition was the critical point of CO_2, which was discovered by Andrews in 1869 [3]. However, the renormalization-group (RG) theory for this transition and other continuous phase transitions in general [4–7] was developed more than a century later, based on the scaling and universality in the critical phenomena appearing near such transitions [8]. Some of the results predicted by this theory have now been determined to high precision, and are consistent with the results of high-quality microgravity experiments [9].

FOPTs, on the other hand, were apparently recognized far earlier and appear far more frequently in nature [10–13]. Take H_2O as an example. The conventional phase diagram of this material contains three phases: ice, water, and vapor, which are commonly encountered in the normal environment. All transitions between these phases are FOPTs, except for the isolated critical point at the end of the line of vaporization. The first well-known theory of phase transitions is van der Waals' equation of state [14], which provides a description of the critical point and, when combined with Maxwell's equal-area construction [15], predicts that a gas–liquid coexistence region exists [15]. Within this gas–liquid coexistence region, metastable and unstable states are separated by a well-defined spinodal curve, at which the isothermal compressibility diverges. Gibbs' theory of equilibrium [16] further identifies two distinct mechanisms of equilibration for the two kinds of nonequilibrium states, viz., nucleation and growth [17–19] versus unstable growth (or spinodal decomposition [20], which is often discussed with regard to binary systems). This picture of the FOPTs has dominated their study for more than a cen-

*arXiv: 1205.1400.

tury. Indeed, a specific theory of nucleation is still held in high regard at present, despite the fact that the nucleation rate predicted by this theory agrees with measured values to within several orders of magnitude only [18, 19]. Further, the nonlinear theory of spinodal decomposition [21] has yet to be substantially improved [20]. The only modification that has been made to the FOPT picture is the belief that the crossover of the two transition modes is smooth rather than sharp and, thus, the spinodal curve (if it exists) is not sharp [22–24]. In addition, metastable and unstable states are often accompanied by hysteresis, a non-equilibrium and nonlinear phenomenon that is difficult to control. Accordingly, a general theory that is comparable to the well-developed framework of the RG theory for continuous transitions has yet to be developed for FOPTs.

A challenging question along this line of investigation is whether scaling and universality exist in FOPTs, because such behavior may be employed as general characteristics in the study of FOPTs as an alternative to case studies. In the case of equilibrium, within the framework of the RG theory, it has been argued that the discontinuity of extensive variables across an FOPT corresponds to the existence of a discontinuity fixed point with at least one eigenvalue equal to the system dimensionality [25]. Trivial scaling behavior then follows [26]. From the dynamic perspective, there are two main scenarios for which scaling and universality emerge. One scenario is usually referred to as phase-ordering kinetics, in which a system evolves to an equilibrium thermodynamic state consisting of two coexisting phases from a non-equilibrium metastable or unstable one-phase state, which, in turn, usually originates from rapid quenching of a one-phase, thermal-equilibrium state [10, 11, 27]. In such systems, one finds that the structure function scales by a time-dependent characteristic length scale in the late stages of growth, which characterizes the sizes of the growing domains [28]. Several universality classes have also been established in relation to Models A, B, etc., which were originally defined in critical dynamics [29]. Naturally, the RG theory has been applied to such phase ordering kinetics in order to understand the origin of such dynamic scaling [27]. However, the lack of a small parameter analogous to the critical phenomenon case essentially renders such approaches as scaling analyses [27]. As many practical transitions are driven by an external field or the temperature in such a manner that the systems change completely from one phase to the other, it has been found that the energy dissipations and/or hysteresis exhibit scaling with respect to the field sweep rate, which serves as a characteristic of the irreversible processes involved [30–39].

An RG theory has also been adapted successfully to the dynamic scaling of hysteresis in a toy vector model with an infinite number of vector components and under the influence of a varying external field. Hence, scaling forms determined by a zero-temperature fixed point were obtained with respect to the field sweep rate, agreeing excellently with numerical results [40]. A subsequent attempt to study the scaling in a more practical Ising model using the Monte Carlo RG method has not yet succeeded in determining the fixed point unambiguously [41]. Recently, focusing on the dynamics of a generic FOPT driven by an external field in the ϕ^4 model below its usual critical point, we employed a field-theoretic RG method to show that the scaling behavior of the FOPT is governed by an unexpected instability fixed point of a corresponding φ^3 model. Accordingly, the FOPT exhibits distinct scaling and universality behavior with corresponding instability exponents different from the critical exponents [42].

Here, we follow a more standard approach and conduct a detailed study of a mean-field theory, a Gaussian theory, a perturbation expansion about the mean-field theory, and a field-theoretic RG theory of the φ^3 theory. We also employ the Yang–Lee edge singularity to improve the estimates of the instability exponents. The good agreement of these estimates with existing numerical results, together with the mean-field numerical and analytical outcomes, shows that the FOPT and the third-order transition described by the φ^3 theory are most likely governed by the same instability point and, hence, instability fixed points. This is despite the fact that, in the mean-field theory, the FOPT and the third-order transition described by the φ^3 theory fall into opposite ground states and appear different. We also discuss the manner in which the imaginary fixed points are reached, which is related to the relevancy of the fixed points.

The remainder of this paper is organized as follows. In Section 2, starting with a conventional scalar ϕ^4 model below its critical temperature and in the presence of an external field, we derive an associated φ^3 model that is relevant to the involved FOPTs. The dynamics of the model is also defined. After a brief review of the dynamic field theory to set the stage in Section 3, we present details of the mean-field theory (Section 4), followed by those of the Gaussian theory (Section 5), which describes fluctuations around the mean-field theory and clearly exhibits a divergent correlation length and a divergent correlation time similar to the critical phenomena. The one-loop perturbation expansions, which exhibit infrared divergences below the upper critical dimension of 6, are then discussed in Section 6. Detailed exposition of the RG theory used to manage the divergences is given in Section 7. Then, in Section 8, we argue that the large-scale behavior of the scalar φ^3 theory for FOPTs falls into the same universality class as the Yang–Lee edge singularity [43], and employ its extant exponents to two-

and three-loop approximations, so as to estimate the instability exponents for the FOPTs. As the infrared stable fixed point found for the φ^3 theory is purely based on imaginary numbers, in Section 9 we enter into discussions on concerns about whether the fixed point describes true asymptotic scaling behavior or is just a crossover. A summary is presented in Section 10. Two appendices are included, which briefly sketch the formulation of a supersymmetry dynamic action (Appendix A) and the computations of the relevant integrals and expansions (Appendix B).

2 Model

2.1 Scalar ϕ^4 model

We consider a model with a conventional Ginzburg–Landau functional

$$\mathcal{H}[\phi] = \int \mathrm{d}\boldsymbol{x} \left\{ \frac{1}{2} r\phi^2 + \frac{1}{4!} g\phi^4 + \frac{1}{2}[\nabla\phi]^2 - H\phi \right\} \tag{1}$$

of a scalar-order parameter ϕ in the presence of an external field H, where g is a coupling constant that is positive for stability. Further, $r = c_1(T - T_c)$ is the reduced temperature, with T_c being the mean-field critical temperature and c_1 a positive constant. The total free energy is

$$\mathcal{F} = -\ln Z = -\ln \int \mathcal{D}\phi \exp\{-\mathcal{H}[\phi]\}, \tag{2}$$

where the functional integral is over all possible configurations and we have absorbed the temperature factor into the definition of $\mathcal{H}$. The free energy thus obtained is the true free energy, in the sense that it describes the equilibrium properties of the system in question. Therefore, it ought to be a convex function of the order parameter and, thus, should not possess any metastable or unstable states. Analytical continuation of this free energy to the metastable region induces a complex free energy, the real and imaginary parts of which describe the equilibrium properties of the metastable states and their lifetimes, respectively [44]. On the other hand, in Eq. (2), the free-energy functional or Hamiltonian [Eq. (1)] is itself supposed to be a result of a constrained integration of those fields over a spatial region of size a or, in terms of the spatial Fourier transform,

$$\phi(\boldsymbol{k}) = \int \mathrm{d}\boldsymbol{x}\phi(\boldsymbol{x}) \exp(-\mathrm{i}\boldsymbol{k}\cdot\boldsymbol{x}), \tag{3}$$

for those fields whose wave numbers are larger than a momentum cutoff Λ, which is proportional to $1/a$. This coarse-grained procedure yields a functional possessing both metastable and unstable states and is appropriate to describe their dynamical properties [45–47]. Note that we have used the same symbol for both direct and Fourier transformed spaces in Eq. (3). We shall employ this approach throughout the paper.

2.2 Derived φ^3 model

We shall study the FOPTs in the model expressed in Eq. (1) and, thus, shall take $r < 0$ throughout the paper. It is well known that there is a spatially uniform spontaneous magnetization M (in the terminology employed in the study of magnetism) below T_c, even in the absence of H. Accordingly, it is essential to shift the order parameter by M. In particular, let

$$\phi = M + \varphi. \tag{4}$$

Then,

$$\begin{aligned}\mathcal{H}[\varphi] = {} & V(rM^2/2 + gM^4/4! - HM) \\ & + \int \mathrm{d}\boldsymbol{r} \left[\frac{1}{2}\tau\varphi^2 + \frac{1}{3!} g_3\varphi^3 + \frac{1}{4!} g\varphi^4 \right. \\ & \left. + \frac{1}{2}(\nabla\varphi)^2 - h\varphi \right],\end{aligned} \tag{5}$$

where V is the volume of the system,

$$\tau = r + \frac{1}{2} gM^2, \quad h = H - rM - \frac{1}{3!} gM^3, \tag{6}$$

and

$$g_3 = gM. \tag{7}$$

Later, we shall show that the long-wavelength behavior of the system is dominated by the leading φ^3 term in Eq. (5) [42]. Therefore, neglecting the φ^4 term, we have derived a φ^3 model, where [42]

$$\mathcal{H}_3[\varphi] = \int \mathrm{d}\boldsymbol{r} \left(\frac{1}{2}\tau\varphi^2 + \frac{1}{3!} g_3\varphi^3 + \frac{1}{2}[\nabla\varphi]^2 - h\varphi \right). \tag{8}$$

Note that a φ^3 model has been noted in an RG analysis of a mean-field spinodal fixed point [48], and has also been used in a nucleation theory for systems with long-range interactions near the mean-field spinodal point [49, 50]. However, these theories are of mean-field nature only. In contrast, we shall take fluctuations into account.

2.3 Dynamics

Metastability is essentially kinetic in origin. In order to handle this behavior, we consider a phenomenological dynamics governed by the Langevin equation

$$\frac{\partial\phi}{\partial t} = -\lambda \frac{\delta\mathcal{H}[\phi]}{\delta\phi} + \zeta, \tag{9}$$

i.e., Model A in the critical dynamics case [29], with a Gaussian white noise ζ satisfying

$$\langle\zeta(\boldsymbol{x},t)\rangle = 0,$$
$$\langle\zeta(\boldsymbol{x},t)\zeta(\boldsymbol{x'},t')\rangle = 2\lambda\delta(\boldsymbol{x}-\boldsymbol{x'})\delta(t-t'), \tag{10}$$

or, equivalently, satisfying a local functional probability distribution

$$\mathcal{D}\rho(\zeta) = \mathcal{D}\zeta\exp\left[-\frac{1}{4\lambda}\int \mathrm{d}\boldsymbol{x}\mathrm{d}t\zeta^2(\boldsymbol{x},t)\right], \tag{10'}$$

where λ is a kinetic coefficient. The noise is intended to mimic the effects on the order parameter of those integrated degrees of freedom having short relaxation times. Accordingly, there also exists a coarse-grained time scale, in principle, and, hence, a cutoff frequency. Nevertheless, we shall neglect this constraint in what follows, as we shall consider sufficiently long-time universal behavior.

3 Dynamical field theory

The solution ϕ of the dynamic equations (9) and (10) depends on ζ and is, thus, stochastic and ought to be averaged over the distribution given in Eq. (10′). The standard practice is to formulate the problem in terms of a dynamical field theory [51–56], because standard field-theoretic techniques then become applicable. We shall briefly repeat the main steps leading to the dynamic action in Section 3.1. In addition, we will collect the definitions of the generating functionals for connected Green functions and vertex functions and discuss their relation in Section 3.2. The formulation of the theory in a supersymmetric form is left to Appendix A, which serves also to indicate the supersymmetric origin of some of the relations.

3.1 Dynamic action

A convenient method of obtaining the required averages is to calculate the generating functional, defined as

$$Z[J] = \left\langle\exp\left[\int \mathrm{d}\boldsymbol{x}\mathrm{d}tJ(\boldsymbol{x},t)\phi(\boldsymbol{x},t)\right]\right\rangle, \tag{11}$$

where the angle brackets denote the average over ζ. Then, quantities of interest such as the magnetization and n-point correlation functions are readily obtainable via derivation with respect to the external source J, such that

$$C_1(x) \equiv \langle\phi(x)\rangle = \frac{1}{Z[0]}\frac{\delta Z}{\delta J(x)}\bigg|_{J=0}, \tag{12}$$

$$C_n(x_1,\ldots,x_n) \equiv \langle\phi(x_1)\ldots\phi(x_n)\rangle = \frac{1}{Z[0]}\frac{\delta^n Z}{\delta J(x_1)\ldots\delta J(x_n)}\bigg|_{J=0}, \tag{13}$$

where we use x_n to denote $(\boldsymbol{x}_n,t_n)$.

The condition that ϕ must be the solution of Eq. (9) can be fulfilled by inserting a Dirac delta function in Eq. (11), which may in turn be represented by a functional Fourier transform through introduction of an auxiliary response field $\tilde{\phi}$ [57]. Therefore,

$$Z[J] = \int \mathcal{D}\rho(\zeta)\mathcal{D}\phi\mathcal{D}\tilde{\phi}\mathcal{J} \times\exp\left\{\int \mathrm{d}\boldsymbol{x}\mathrm{d}t\left[J\phi+\tilde{\phi}\left(\zeta-\frac{\partial\phi}{\partial t}-\lambda\frac{\delta\mathcal{H}}{\delta\phi}\right)\right]\right\}, \tag{14}$$

where the integration over $\tilde{\phi}$ runs along the imaginary axis, and $\mathcal{J}$, given formally by

$$\mathcal{J} = \det\left[\frac{\mathcal{D}\zeta}{\mathcal{D}\phi}\right] = \det\left[\left(\frac{\partial}{\partial t}+\lambda\frac{\delta^2\mathcal{H}}{\delta\phi^2}\right)\right], \tag{15}$$

is the functional Jacobian for transformation to the integration over ϕ. Here, det denotes the determinant. Integrating over the noise leads to

$$Z[J,\tilde{J}] = \int \mathcal{D}\phi\mathcal{D}\tilde{\phi}\mathcal{J}\exp\left[-\mathcal{L}+\int \mathrm{d}\boldsymbol{x}\mathrm{d}t(J\phi+\tilde{J}\tilde{\phi})\right], \tag{16}$$

with the action $\mathcal{L}$ given by

$$\mathcal{L} = \int \mathrm{d}\boldsymbol{x}\mathrm{d}t\left[\tilde{\phi}\left(\frac{\partial\phi}{\partial t}+\lambda\frac{\delta\mathcal{H}}{\delta\phi}\right)-\lambda\tilde{\phi}^2\right]. \tag{17}$$

We have inserted another source $\tilde{J}$ conjugate to $\tilde{\phi}$ in Eq. (16), such that the response functions that are averages of the $\tilde{\phi}$ and ϕ fields can be calculated via a method similar to that shown in Eq. (13). In particular, the two-point response function $G_{11}(x,x') = \langle\phi(x)\tilde{\phi}(x')\rangle$ is

$$G_{11}(x,x') = \frac{1}{Z[0,0]}\frac{\delta^2 Z[J,\tilde{J}]}{\delta J(x)\delta\tilde{J}(x')}\bigg|_{\substack{J=0\\ \tilde{J}=0}} = \frac{1}{\lambda}\frac{\delta\langle\phi(x)\rangle}{\delta H(x')}, \tag{18}$$

which is obtained by noting that an external field is equivalent to the source $\tilde{J}$ up to λ. The last equality of Eq. (18) expresses the response to an external field and is, therefore, the justification for referring to $\tilde{\phi}$ as the response field. The response field in Eq. (17) may be integrated out via a Gaussian integral; however, the resultant functional is nonlinear and inconvenient for treatment.

At this point, two different methods can be used to continue tackling the Jacobian (15), which yield two different forms of action. We shall proceed with the conventional approach and leave the more exotic method to Appendix A.

The conventional method is to note that the determinant [51, 53, 55]

$$\mathcal{J} = \exp\left[\Theta(0)\lambda \int \mathrm{d}\boldsymbol{x}\mathrm{d}t \frac{\delta^2 \mathcal{H}}{\delta\phi^2}\right] \equiv \exp\left(-\mathcal{L}'\right), \tag{19}$$

where the Heaviside step function defined as

$$\Theta(t) = \begin{cases} 1, & t > 0 \\ -1, & t < 0 \end{cases} \tag{20}$$

must be assigned a special value $\Theta(0) = 1/2$ for consistency in the continuum limit of a symmetrized discretization of the Langevin equation [52, 53, 55]. Therefore, one obtains a dynamical field theory with a total action $\mathcal{L}_{\mathrm{tot}} = \mathcal{L} + \mathcal{L}'$. Standard field theoretical methods can then be utilized to compute the relevant response functions. In particular, Feynman rules for perturbation expansions may be defined (see Section 6 below). One can then prove that diagrams with a closed response loop given by contraction of ϕ and $\tilde{\phi}$ at the same spatial-temporal point [i.e., both ϕ and $\tilde{\phi}$ come from the same term $\lambda\tilde{\phi}\delta\mathcal{H}/\delta\phi$ in Eq. (17)] yield $\lambda G(0)\delta^2\mathcal{H}/\delta\phi^2 = -\mathcal{L}'$ only and, thus, simply cancel the Jacobian exactly for each order of the perturbation expansions, because $G(0) = \Theta(0)$ [see Eq. (75) below]. As a consequence, one may simply ignore the Jacobian by choosing $\Theta(0) = 0$ [51, 52, 55], which corresponds to a forward discretization, and, meanwhile, excludes closed response loops from the perturbation expansions. Note that, in this manner,

$$Z[J,\tilde{J}] = \int \mathcal{D}\phi\mathcal{D}\tilde{\phi} \exp\left[-\mathcal{L} + \int \mathrm{d}\boldsymbol{x}\mathrm{d}t(J\phi + \tilde{J}\tilde{\phi})\right] \tag{21}$$

in the ensuing dynamical field theory, with the dynamic action given by Eq. (17). Causality is then automatically implemented, because [51, 58]

$$\langle \phi(t_1)\ldots\phi(t_n)\tilde{\phi}(t'_1)\ldots\tilde{\phi}(t'_{n'})\rangle = 0, \quad \text{if one } t'_{i'} > \text{all } t_i. \tag{22}$$

In particular,

$$\langle \tilde{\phi}(t'_1)\ldots\tilde{\phi}(t'_{n'})\rangle = 0. \tag{23}$$

3.2 Connected Green functions and vertex functions

From $Z[J,\tilde{J}]$, Eq. (21) (or the partition function in statistical mechanics, as it may be regarded as defining the statistical weight of a $(\phi,\tilde{\phi})$ configuration), one defines another generating functional $W[J,\tilde{J}]$, the minus free energy, where

$$W[J,\tilde{J}] = \ln Z[J,\tilde{J}], \tag{24}$$

for connected correlation and response functions, or the cumulants

$$\begin{aligned} &G^c_{nn'}(x_1,\ldots,x_n,x'_1,\ldots,x'_{n'}) \\ &\equiv \langle\phi(x_1)\ldots\phi(x_n)\tilde{\phi}(x'_1,\ldots,x'_{n'})\rangle_c \\ &= \left.\frac{\delta^{n+n'}W[J,\tilde{J}]}{\delta J(x_1)\ldots\delta J(x_n)\delta\tilde{J}(x'_1)\ldots\tilde{J}(x'_{n'})}\right|_{\substack{J=0\\ \tilde{J}=0}}, \end{aligned} \tag{25}$$

which are generally deviations and their moments. For example, the connected two-point correlation function

$$\begin{aligned} G^c_{20}(x,x') &= \langle[\phi(x)-\langle\phi\rangle][\phi(x')-\langle\phi\rangle]\rangle \\ &= C_2(x,x') - \langle\phi\rangle^2 \equiv C(x,x'), \end{aligned} \tag{26}$$

is the second moment of the deviation $\phi - \langle\phi\rangle$. Accordingly, one may construct the correlation and response functions from their connected counterparts, the Feynman diagrams of which are fewer in number at high orders in perturbation expansions.

The connected diagrams contain one-line reducible and irreducible diagrams, which are distinguished based on whether or not they are connected when an internal line of the diagrams is cut. The former are products of the latter, which can be proven to be generated by the Gibbs free energy Γ through a Legendre transformation, such that

$$\Gamma[\langle\tilde{\phi}\rangle,\langle\phi\rangle] = -W[J,\tilde{J}] + \int \mathrm{d}\boldsymbol{x}\mathrm{d}t\left(J\langle\phi\rangle + \tilde{J}\langle\tilde{\phi}\rangle\right), \tag{27}$$

where $\langle\phi\rangle$ and $\langle\tilde{\phi}\rangle$ are averages in the presence of J and $\tilde{J}$ and are given by

$$\langle\phi\rangle \equiv \frac{\delta W}{\delta J}, \quad \langle\tilde{\phi}\rangle \equiv \frac{\delta W}{\delta\tilde{J}}. \tag{28}$$

Then, from Eqs. (27) and (28),

$$J = \frac{\delta\Gamma}{\delta\langle\phi\rangle}, \quad \tilde{J} = \frac{\delta\Gamma}{\delta\langle\tilde{\phi}\rangle}, \tag{29}$$

and the one-line irreducible vertex function $\Gamma_{n'n}$ is

$$\begin{aligned} &\Gamma_{n'n}(x'_1,\ldots,x'_{n'},x_1,\ldots,x_n) \\ &= \left.\frac{\delta^{n'+n}\Gamma[\langle\tilde{\phi}\rangle,\langle\phi\rangle]}{\delta\langle\tilde{\phi}(x'_1)\rangle\ldots\delta\langle\tilde{\phi}(x'_{n'})\rangle\delta\langle\phi(x_1)\rangle\ldots\delta\langle\phi(x_n)\rangle}\right|_{\substack{J=0\\ \tilde{J}=0}}. \end{aligned} \tag{30}$$

In particular, differentiating Eq. (29) with J and $\tilde{J}$ and

employing Eqs. (25) and (26) yields

$$\Gamma_{02}(x_1,x_2)=0, \tag{31}$$

$$\int \mathrm{d}x\Gamma_{11}(x_1,x)G_{11}(x,x_2)=\delta(x_1-x_2), \tag{32}$$

$$\begin{aligned}\int \mathrm{d}x\Gamma_{20}(x_1,x)G_{11}(x,x_2)&\\ =-\int \mathrm{d}xG^c_{20}(x_1,x)\Gamma_{11}(x,x_2)&\\ =-\int \mathrm{d}xC(x_1,x)\Gamma_{11}(x,x_2),&\end{aligned} \tag{33}$$

where the first equation is a result of Eq. (23) and use has been made of the relation $G^c_{11}=G_{11}$ resulting from Eq. (23). In addition, the fluctuation-dissipation theorem

$$\lambda[G_{11}(x,x')-G_{11}(x',x)]=-\frac{\partial C(x,x')}{\partial t} \tag{34}$$

holds, relating the response function to the correlation function [51, 53–56, 59, 60]. Moreover, the dynamic response functions converge to their corresponding static correlation functions over long time periods [51, 53, 54, 60]. In fact, these are consequences of the supersymmetry in the theory [53].

4 Mean-field theory

In this section, we study the mean-field theory of a field-driven FOPT and show that it is controlled by an instability point [42], which corresponds to the spinodal point in the mean-field theory.

4.1 φ^3 model and instability point

The mean-field theory is the lowest order of a saddle-point approximation to the free energy [Eq. (2)]. Assuming that the saddle point lies at a uniform order parameter, the magnetization M, we obtain the free energy density

$$F=\mathcal{F}/V=\mathcal{H}/V=\frac{1}{2}rM^2+\frac{1}{4!}gM^4-HM. \tag{35}$$

The dynamics then reduces to

$$\frac{\mathrm{d}M}{\mathrm{d}t}=-\lambda\left(rM+\frac{1}{3!}gM^3-H\right), \tag{36}$$

from Eqs. (9) and (35). It is well known that a mean-field critical point exists at $r=0$ and $H=0$; the mean-field critical exponents of this point are collected in Table 1 for later comparison. For $r<0$, on the other hand, an equilibrium FOPT exists at $H=0$ between the two phases, with $M=\pm\sqrt{-6r/g}\equiv\pm M_e$ for each given r and g. As there is no fluctuation, the FOPT cannot occur at the equilibrium transition point at $H=0$, because there is a free-energy barrier of $|F(0)-F(M_e)|=3r^2/(2g)$ between the two phases. Rather, the FOPT can only occur beyond the point at which the barrier vanishes. In fact, this point corresponds to the spinodal point at which both the first and second derivatives of F with respect to M vanish.

To see the essence of this transition, let us set $M=M_s+m(t)$ in Eq. (36), which becomes

$$\frac{\mathrm{d}m}{\mathrm{d}t}=-\lambda\left(\tau m+\frac{1}{2}gM_sm^2+\frac{1}{3!}gm^3-h\right), \tag{37}$$

where M_s is a constant and

$$\tau=r+\frac{1}{2}gM_s^2,\quad h=H-rM_s-\frac{1}{3!}gM_s^3, \tag{38}$$

which corresponds simply to Eq. (6) at M_s. We find a pair of spinodal points lying at

$$\tau_s=0,\quad h_s=0, \tag{39}$$

or, from Eq. (38), at $M_s=\pm\sqrt{-2r/g}$ and $H_s=\mp(2r/3)\sqrt{-2r/g}$. Accordingly, Eq. (38) can be expressed as

$$\tau=c_1(T-T_s),\quad h=H-H_s, \tag{40}$$

with $T_s=T_c-gM_s^2/(2c_1)$ at either point. Through comparison with Eq. (36), it becomes apparent that each point at its associated transition plays a similar role to the critical point. The only difference is that one has a quadratic term in Eq. (37). However, m is small in the vicinity of the spinodal point. This term overwhelms the cubic term and, thus, controls the dynamics. Therefore, upon neglecting the cubic term in Eq. (37), the dynamics in the vicinity of the spinodal point becomes

$$\frac{\mathrm{d}m}{\mathrm{d}t}=-\lambda\left(\tau m+\frac{1}{2}gM_sm^2-h\right), \tag{41}$$

which is governed by the derived φ^3 model, Eq. (8). The corresponding mean-field free energy density of this model is

$$F_3=\frac{1}{2}\tau m^2+\frac{1}{3!}gM_sm^3-hm. \tag{42}$$

Further, each spinodal point [Eq. (39)] now becomes the instability point of the $m=0$ state, because the system becomes unstable at these points, as can be seen in Fig. 1(a).

Note that we return to the ϕ^4 theory if we neglect the quadratic term in Eq. (37). However, the critical point would then be replaced by one of the two spinodal

points. This is the theory of pseudo-critical phenomena, for which conventional critical behavior emerges at the spinodal point rather than the critical point [61]. However, in this case, the critical fixed point is unstable against the neglected quadratic term and only crossover may be observed [61].

4.2 Mean-field static instability exponents

As the free energy of the φ^3 model is known, one can then derive its associated exponents, similar to the ϕ^4 mean-field model. We refer to these exponents as "instability exponents" or even "spinodal exponents," as they are associated with the instability point or spinodal point. It will become apparent that these exponents are the exact counterparts of the critical exponents. Accordingly, we shall use identical symbols to those used for the critical exponents.

At equilibrium, Eq. (41) yields the equation of state

$$\tau m + \frac{1}{2} g M_s m^2 = h. \tag{43}$$

As a result,

$$m = \begin{cases} 0, & \tau > 0, \\ -2\tau/(gM_s) \sim (T_s - T)^{\beta}, & \tau < 0, \end{cases} \tag{44}$$

for $h = 0$. Therefore, m changes continuously to zero with $\beta = 1$. Also, as $h \sim m^2$ at $\tau = 0$, $\delta = 2$. Differentiating Eq. (43) yields

$$\chi = \left.\frac{\partial m}{\partial h}\right|_{h=0} = \begin{cases} \tau^{-1} \sim (T - T_s)^{-\gamma}, & \tau > 0, \\ (-\tau)^{-1} \sim (T_s - T)^{-\gamma'}, & \tau < 0, \end{cases} \tag{45}$$

for the susceptibility. Thus, $\gamma = \gamma' = 1$, with these terms being identical to their critical counterparts. However, the amplitude ratio between the susceptibility above and below $\tau = 0$ is now 1 instead of 2. The free energy density for the two solutions is

$$F_3 = \begin{cases} 0, & \tau > 0, \\ 2\tau^3/(3g^2 M_s^2), & \tau < 0. \end{cases} \tag{46}$$

Thus, the specific heat is

$$C = -T\frac{\partial^2 F_3}{\partial T^2} = \begin{cases} 0, & \tau > 0, \\ -4\tau c_1^2 T/(g^2 M_s^2) \sim (T_s - T)^{-\alpha}, & \tau < 0, \end{cases} \tag{47}$$

which again changes continuously from one state to the other with $\alpha = -1$. Note that these instability exponents are also collected in Table 1.

Table 1 Mean-field critical and instability exponents.

Theory	d_c	β	δ	γ	α	ν	η	z	n_H	n_m
ϕ^4	4	$\frac{1}{2}$	3	1	0	$\frac{1}{2}$	0	2	$\frac{3}{5}$	$\frac{1}{5}$
φ^3	6	1	2	1	-1	$\frac{1}{2}$	0	2	$\frac{2}{3}$	$\frac{1}{3}$

A caveat is required here. It is apparent from Eq. (44) and Fig. 1(a) that the instability exponents just derived describe the continuous transition from the state with $m = -2\tau/(gM_s)$ to that with $m = 0$. As the specific heat is linear in τ, from Eq (47), this is, in fact, a third-order phase transition in the classical classification [1]. We must then ask if this transition is related to the FOPT we are attempting to study. The answer is yes, as can be seen from Fig. 1(b). As mentioned above, there are two transitions associated with two spinodal points (indicated by stars in Fig. 1(c)), which are related via inversion symmetry. Without loss of generality, let us consider the transition with positive M_s and negative H_s. The FOPT is then driven by increasing H in the direction opposite to M_s, as shown in Fig. 1(c). This corresponds to a positive gM_s, with h changing from positive to negative, as shown in Fig. 1(b). Provided $0 > H > H_s$ and, hence, $h = H - H_s > 0$, the system remains in the metastable state with $M > 0$. This corresponds to the scenario in which m resides in a well. As h decreases, the well becomes shallower and closer to the origin. At exactly $h = 0$, the system lies at the transition point and becomes unstable. For $h < 0$, the positive m state loses its stability and, eventually, falls to negative infinity. In practice, of course, the system restabilizes at a negative M, because of the neglected quartic term in the free energy when m becomes large (negative). Thus, the exponents are, in fact, the properties of the transition point at $h = 0$, rather than the well at $h > 0$. This becomes apparent in the RG theory of the critical phenomena and, also, of the FOPTs, as will be seen below. In this theory, the exponents are properties

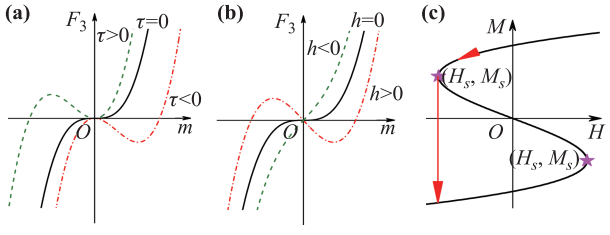

Fig. 1 φ^3 mean-field free-energy density for **(a)** three different τ at $h = 0$ and **(b)** three different h at $\tau = 0$. **(c)** Generic hysteresis of the ϕ^4 model in an external field H. The arrows depict the transition that can be described by (b). The stars mark the spinodal/instability points.

of a fixed point. Only the critical point of a real system converges upon renormalization to the fixed point, not the equilibrium phase. This behavior indicates that the RG is insensitive to the minima, which are a finite distance away [62]. This is despite the fact that doubt was cast on this argument [62], which arose from the RG study of the Potts model, the Landau mean-field theory of which predicts an FOPT instead of a continuous transition [63]. Nevertheless, in this paper, we shall show that the instability point does describe the FOPT. However, for the FOPT we consider here, the system falls towards the unstable left side instead of the right well. This may explain why the fixed point we find below is imaginary [42].

4.3 Mean-field hysteresis exponents and their verification

We now show that the mean-field instability exponents are indeed relevant to the considered FOPTs.

In order to probe these exponents, we utilize the method of finite-time scaling proposed for critical phenomena [64, 65], in which H is swept linearly through the instability point. To be specific, we again consider the transition depicted in Fig. 1(c) and assume that

$$h = -Rt \quad \text{or} \quad H = H_s - Rt, \tag{48}$$

where R is a constant. This form of driving implies the choice of $t = 0$ at $h = 0$. In fact, one can begin sweeping the field from anywhere sufficiently far from H_s; for example, $H = H_0 - Rt$. However, $h = 0$ always shifts the time origin to the time at H_s, i.e., $h = -R(t - t_s)$, which recovers Eq. (48) upon setting $t_s = 0$. The linear driving imposes an effective finite time scale on the system, which is proportional to R^{-z/r_H}, where r_H, the RG eigenvalue associated with R, satisfies

$$r_H = z + \beta\delta/\nu \tag{49}$$

with z and ν being instability exponents. When this driving time scale is shorter than the correlation time, finite-time scaling follows. This behavior is in close analogy to the occurrence of finite-size scaling when the system size is smaller than its correlation length. In Section 7.7 below, we show that m follows a finite-time scaling form of

$$m(h, R) = R^{\beta/(\nu r_H)} f(-hR^{-\beta\delta/(\nu r_H)}), \tag{50}$$

near the instability point $\tau = 0$ and $h = 0$, where f is a scaling function. Using the mean-field instability exponents derived in the last section and those that will be derived in the next section, all collected in Table 1, one finds that Eq. (50) becomes

$$m(h, R) = R^{1/3} f(-hR^{-2/3}). \tag{51}$$

This means that, at $m = 0$ or $M = M_s$, the transition field is expressed as

$$h_t \equiv H_t - H_s = c_2 R^{2/3} \sim R^{n_H} \tag{52}$$

and, at $h = 0$, the transition moment is

$$m_t(0, R) \equiv M_t - M_s = f(0) R^{1/3} \sim R^{n_m}, \tag{53}$$

where c_2 is the root of f, i.e., $f(-c_2) = 0$, and $n_H = \beta\delta/(\nu r_H) = 2/3$ and $n_m = \beta/(\nu r_H) = 1/3$ are hysteresis exponents [42]. All these results are supported by the direct numerical solutions of Eq. (36) shown in Fig. 2. Note that, if the original ϕ^4 theory rather than the φ^3 theory governs the transition, the critical exponents listed in Table 1 give $n_H = 3/5$ and $n_m = 1/5$ [66], which can be excluded from Fig. 2. This result indicates that the theory of pseudo-critical phenomena [61] cannot describe the mean-field theory, at least.

In fact, the above results can even be proven analytically. Equation (41) is a kind of Riccati equation that can be solved analytically [67]. For the driving (Eq. (48)) and $\tau = 0$,

$$m = \frac{2}{gM_s\lambda y}\frac{\mathrm{d}y}{\mathrm{d}t} \quad \text{and} \quad s = \sqrt[3]{gM_s\lambda^2 R/2}\, t \tag{54}$$

transform Eq. (41) into the Airy equation

$$\frac{\mathrm{d}^2 y}{\mathrm{d}s^2} = sy, \tag{55}$$

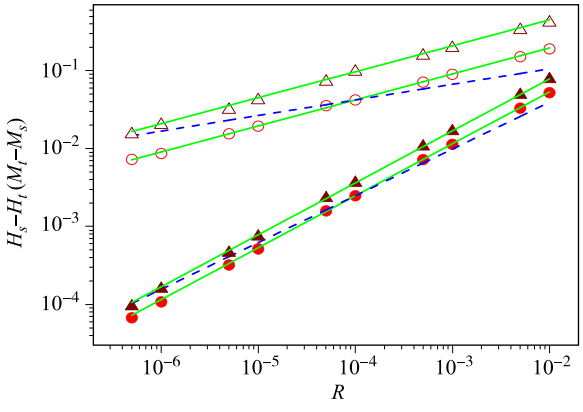

Fig. 2 Mean-field transition fields $H_s - H_t$ (*filled symbols*) and moments $M_t - M_s$ (*opened symbols*) versus R. Full lines through filled symbols and opened symbols are lines of slopes 2/3 and 1/3, respectively, through the data points at $R = 10^{-4}$. The two dashed lines have slopes 3/5 (*lower*) and 1/5 (*upper*) for comparison. Note that the symbols have small vertical variations due to the interpolations in extracting the points but can never fit the dashed lines. The parameters chosen are $r = -1$, $\lambda = 1$, and $g = 1$ (*circles*) and $g = 0.1$ (*triangles*).

which is solved using the Airy functions Ai and Bi, to yield

$$y = c_3 Ai(s) + c_4 Bi(s), \tag{56}$$

where c_3 and c_4 are constants to be determined based on initial conditions. Consequently,

$$m(t) = \sqrt[3]{\frac{4R}{g^2\lambda}}\frac{c_3 Ai'(\sqrt[3]{g\lambda^2 R/2}t) + c_4 Bi'(\sqrt[3]{g\lambda^2 R/2}t)}{c_3 Ai(\sqrt[3]{g\lambda^2 R/2}t) + c_4 Bi(\sqrt[3]{g\lambda^2 R/2}t)}, \tag{57}$$

from Eqs. (54) and (56), where the primes indicate a derivative with respect to the argument. Therefore, one recovers Eq. (52) from Eq. (54), with $c_2 = s_t/\sqrt[3]{g\lambda^2/2}$ at $s = s_t$, at which $m = 0$. One also recovers Eq. (53) from Eq. (57) at $h = Rt = 0$, with $f(0) = \sqrt[3]{4/g^2\lambda}[c_3 Ai'(0) + c_4 Bi'(0)]/[c_3 Ai(0) + c_4 Bi(0)]$.

Therefore, these mean-field results clearly show that the dynamic scaling of the hysteresis in the FOPT of the ϕ^4 model is determined by the instability point of the derived φ^3 model.

5 Gaussian theory

In this section, we consider the Gaussian theory for the φ^3 model. This theory, which can be solved analytically, also describes fluctuations in the $m = 0$ state. As a result, the other instability exponents, ν, z, and η, can be derived. More importantly, we shall clearly see that the correlation length and the correlation time both diverge at the instability point, similar to their critical counterparts.

To this end, we use the dynamic action, Eq. (17), which, for $\mathcal{H}_3$ in the absence of the cubic term and h, is expressed as

$$\begin{aligned}\mathcal{L}_0 &= \int \mathrm{d}\boldsymbol{x}\mathrm{d}t\left\{\tilde{\varphi}\left[\frac{\partial\varphi}{\partial t} + \lambda\left(\tau\varphi - \nabla^2\varphi\right)\right] - \lambda\tilde{\varphi}^2\right\}\\ &= \int \mathrm{d}\overline{\boldsymbol{k}}\mathrm{d}\overline{\omega}\{[\mathrm{i}\omega + \lambda(\tau + \boldsymbol{k}^2)]\tilde{\varphi}(\boldsymbol{k},\omega)\varphi(-\boldsymbol{k},-\omega)\\ &\quad -\lambda|\tilde{\varphi}(\boldsymbol{k},\omega)|^2\},\end{aligned} \tag{58}$$

where we have written $\tilde{\varphi}$ in place of $\tilde{\phi}$ for uniformity. The inverse Fourier transform is defined as

$$\varphi(\boldsymbol{x},t) = \int \mathrm{d}\overline{\boldsymbol{k}}\mathrm{d}\overline{\omega}\varphi(\boldsymbol{k},\omega)\exp(\mathrm{i}\boldsymbol{k}\cdot\boldsymbol{x} - \mathrm{i}\omega t), \tag{59}$$

with

$$\int \mathrm{d}\overline{\boldsymbol{k}}\mathrm{d}\overline{\omega} \equiv \frac{1}{(2\pi)^{d+1}}\int \mathrm{d}\boldsymbol{k}\mathrm{d}\omega, \tag{60}$$

where d is the spatial dimensionality. Note that, as we used a finite volume, we should, in principle, replace $[1/(2\pi)^d]\int \mathrm{d}\boldsymbol{k}$ with a discrete sum $(1/V)\sum_{\boldsymbol{k}}$, for consistency. However, a singularity can only emerge in the thermodynamic limit for which $V \to \infty$ and, hence, the sum becomes the continuous integral. Therefore, we continue to use the integral representation. Integrating out both $\tilde{\varphi}$ and φ, we find

$$\begin{aligned}W[J,\tilde{J}] \sim \frac{1}{2}\int \mathrm{d}\overline{\boldsymbol{k}}\mathrm{d}\overline{\omega}[&G(\boldsymbol{k},-\omega)\tilde{J}(-\boldsymbol{k},-\omega)J(\boldsymbol{k},\omega)\\ &+G(\boldsymbol{k},\omega)\tilde{J}(\boldsymbol{k},\omega)J(-\boldsymbol{k},-\omega)\\ &+C(\boldsymbol{k},\omega)J(-\boldsymbol{k},-\omega)J(\boldsymbol{k},\omega)],\end{aligned} \tag{61}$$

from Eq. (24), where we have neglected some irrelevant constants. In Eq. (61),

$$G(\boldsymbol{k},\omega) = \frac{1}{-\mathrm{i}\omega + \lambda(\tau + \boldsymbol{k}^2)}, \tag{62}$$

is related to the two-point response function defined in Eq. (25), according to

$$\begin{aligned}&G_{11}(\boldsymbol{k}_1,\omega_1;\boldsymbol{k}_2,\omega_2)\\ &= \int \mathrm{d}x_1\mathrm{d}x_2 G_{11}(x_1,x_2)\mathrm{e}^{\mathrm{i}\sum_{j=1}^2(\omega_j t_j - \boldsymbol{k}_j\cdot\boldsymbol{x}_j)}\\ &= (2\pi)^{d+1}\delta(\boldsymbol{k}_1 + \boldsymbol{k}_2)\delta(\omega_1 + \omega_2)G(\boldsymbol{k}_1,\omega_1),\end{aligned} \tag{63}$$

with the last equality resulting from translational invariance. Further,

$$\begin{aligned}C(\boldsymbol{k},\omega) &= 2\lambda G(\boldsymbol{k},\omega)G(\boldsymbol{k},-\omega)\\ &= \frac{2\lambda}{\omega^2 + \lambda^2(\tau + \boldsymbol{k}^2)^2}\end{aligned} \tag{64}$$

is related to the two-point correlation function defined in Eq. (26), through a relation similar to Eq. (63). Of course, Eqs. (62) and (64) satisfy the fluctuation-dissipation theorem, Eq. (34), where

$$\lambda[G(\boldsymbol{k},\omega) - G(\boldsymbol{k},-\omega)] = \mathrm{i}\omega C(\boldsymbol{k},\omega) \tag{65}$$

in its Fourier-transformed form. From Eq. (61), we also have

$$G_{02}^c(\boldsymbol{k},\omega) = 0, \tag{66}$$

which is consistent with Eq. (23). As a result, Eqs. (32) and (33) become

$$\begin{aligned}&\Gamma_{11}(\boldsymbol{k},\omega) = G(-\boldsymbol{k},-\omega)^{-1} = \mathrm{i}\omega + \lambda(\tau + \boldsymbol{k}^2) \quad \text{and}\\ &\Gamma_{20}(\boldsymbol{k},\omega) = -\frac{C(\boldsymbol{k},\omega)}{G(\boldsymbol{k},\omega)G(-\boldsymbol{k},-\omega)} = -2\lambda.\end{aligned} \tag{67}$$

In fact, as

$$\begin{aligned}&\langle\varphi(\boldsymbol{k},\omega)\rangle = G(\boldsymbol{k},\omega)\tilde{J}(\boldsymbol{k},\omega) + C(\boldsymbol{k},\omega)J(\boldsymbol{k},\omega) \quad \text{and}\\ &\langle\tilde{\varphi}(\boldsymbol{k},\omega)\rangle = G(\boldsymbol{k},-\omega)J(\boldsymbol{k}\omega)\end{aligned} \tag{68}$$

from Eq. (28), solving to remove J and $\tilde{J}$ and using Eq. (27), we find

$$\begin{aligned}\Gamma = \frac{1}{2}\int \mathrm{d}\overline{\boldsymbol{k}}\mathrm{d}\overline{\omega}[&G(\boldsymbol{k},\omega)^{-1}\langle\tilde{\varphi}(-\boldsymbol{k},-\omega)\rangle\langle\varphi(\boldsymbol{k},\omega)\rangle\\ &+G(\boldsymbol{k},-\omega)^{-1}\langle\tilde{\varphi}(\boldsymbol{k},\omega)\rangle\langle\varphi(-\boldsymbol{k},-\omega)\rangle\\ &-2\lambda\langle\tilde{\varphi}(-\boldsymbol{k},-\omega)\rangle\langle\tilde{\varphi}(\boldsymbol{k},\omega)\rangle],\end{aligned} \tag{69}$$

which recovers Eq. (67) correctly via Eq. (30). Combining Eqs. (65) and (67), we can write the fluctuation-dissipation theorem in the form

$$i\omega\Gamma_{20}(\boldsymbol{k},\omega) = \lambda[\Gamma_{11}(\boldsymbol{k},-\omega) - \Gamma_{11}(\boldsymbol{k},\omega)], \tag{70}$$

or

$$\Gamma_{20}(\boldsymbol{k},\omega) = -\frac{2\lambda}{\omega}\mathrm{Im}\Gamma_{11}(\boldsymbol{k},\omega), \tag{71}$$

which is, of course, satisfied by the Gaussian results.

Equation (62) implies a relaxation or correlation time $t_{\mathrm{eq}}(\boldsymbol{k})$ satisfying

$$\lambda t_{\mathrm{eq}}(\boldsymbol{k}) = (\tau + \boldsymbol{k}^2)^{-1} = \xi^z f_1(\boldsymbol{k}\xi), \tag{72}$$

where

$$\xi = \tau^{-1/2} \sim \tau^{-\nu} \tag{73}$$

is a correlation length and

$$f_1(x) = \frac{1}{1+x^2} \tag{74}$$

is a scaling function with the instability exponents $\nu = 1/2$ and $z = 2$. Indeed, the temporal Fourier transform of Eq. (62) gives

$$G(\boldsymbol{k},t) = \Theta(t)\mathrm{e}^{-\lambda(\tau+\boldsymbol{k}^2)t} = \Theta(t)\mathrm{e}^{-t/t_{\mathrm{eq}}(\boldsymbol{k})}, \tag{75}$$

from the residue theorem, if we note that $G(\boldsymbol{k},\omega)$ has a pole on the negative imaginary ω axis. Therefore, the correlation decays away after $t_{\mathrm{eq}}(\boldsymbol{k})$. Consequently, $G(\boldsymbol{k},\omega)$ can be cast in a scaling form [29]

$$G(\boldsymbol{k},\omega) = \xi^{2-\eta} f_2(\boldsymbol{k}\xi, (\omega/\lambda)\xi^z)/\lambda, \tag{76}$$

with $\eta = 0$ and the scaling function

$$f_2(x,y) = \frac{1}{1 - \mathrm{i}y + x^2}, \tag{77}$$

where the additional λ arises from the time unit. $C(\boldsymbol{k},\omega)$ and $\Gamma_{11}(\boldsymbol{k},\omega)$ can also be expressed in similar forms. Note that $t_{\mathrm{eq}}(\boldsymbol{k})$ diverges for $|\boldsymbol{k}| \to 0$ and $\tau = 0$, similar to ξ.

As pointed out above, relations exist between the dynamic and static functions. It is apparent from Eqs. (62) and (32) that the dynamic functions are equivalent to the static functions up to the kinetic coefficient at $\omega = 0$ or the long-time limit, which is true beyond the Gaussian theory. Thus,

$$\lambda G(\boldsymbol{k},0) = G^{\mathrm{st}}(\boldsymbol{k}) = \frac{1}{\tau + \boldsymbol{k}^2}, \tag{78}$$

where $G^{\mathrm{st}}(\boldsymbol{k})$ is the static correlation function indicated by the superscript. Its inverse Fourier transforms at $d = 3$ and at $\tau = 0$ are proportional to $\exp(-\sqrt{\tau}|\boldsymbol{k}|)$ and $|\boldsymbol{x}|^{d-2}$, respectively, and, hence, confirm Eq. (73) and $\eta = 0$ once more. These kinds of relations can be used as a check of the resultant vertex functions in the dynamics, as will be seen in the following sections.

Note that the Gaussian theory is, in fact, identical for both the ϕ^4 and φ^3 theories. This is the reason why the exponents derived in this section are also identical.

6 Perturbation expansions

Now, we consider the entire model given in Eq. (8). After Fourier transformation, its associated dynamic action becomes

$$\mathcal{L} = \mathcal{L}_0 + \frac{1}{2}g_3'\int \mathrm{d}\overline{\boldsymbol{k}}\mathrm{d}\overline{\boldsymbol{k}'}\mathrm{d}\overline{\omega}\mathrm{d}\overline{\omega'}\tilde{\varphi}(\boldsymbol{k},\omega)\varphi(\boldsymbol{k}',\omega')\varphi(-\boldsymbol{k}-\boldsymbol{k}',-\omega-\omega') - \lambda\int \mathrm{d}\overline{\boldsymbol{k}}\mathrm{d}\overline{\omega}\tilde{\varphi}(-\boldsymbol{k},-\omega)h(\boldsymbol{k},\omega), \tag{79}$$

where $\mathcal{L}_0$ is given by Eq. (58) and $g_3' = \lambda g_3$. The standard method of handling Eq. (79) is to establish perturbation expansions using Feynman diagrams. One observes that λh plays the role of $\tilde{J}$ when comparing Eq. (79) with Eq. (16). Accordingly, we do not take λh as an element of the expansions but, rather, regard it as a specific value of $\tilde{J}$. On the basis of the Gaussian theory, we allow a line, a dashed line, and a filled circle to represent φ, $\tilde{\varphi}$, and -2λ, respectively. Then,

$G(\boldsymbol{k},-\omega) =$ 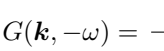 , $C(\boldsymbol{k},\omega) =$ 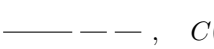 , $-\frac{1}{2}g_3'\delta\left(\sum_{i=1}^{3}\boldsymbol{k}_i\right)\delta\left(\sum_{i=1}^{3}\omega_i\right) =$ 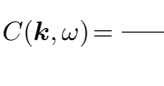 , $-2\lambda =$. (80)

Accordingly, to one-loop order,

$$\Gamma_{10}(\boldsymbol{k},\omega) = \text{-}\bigcirc\text{-} = \frac{1}{2}g_3'(2\pi)V\delta(\boldsymbol{k})\delta(\omega)\int \mathrm{d}\overline{\boldsymbol{k}'}\mathrm{d}\overline{\omega'}C(\boldsymbol{k}',\omega') = \frac{1}{2}g_3'(2\pi)V\delta(\boldsymbol{k})\delta(\omega)\int \mathrm{d}\overline{\boldsymbol{k}'}\frac{1}{\tau+\boldsymbol{k}'^2}, \tag{81}$$

$$\Gamma_{11}(\boldsymbol{k},\omega) = \text{---} + \text{-}\diamond\text{-} = \mathrm{i}\omega + \lambda(\tau+\boldsymbol{k}^2) - g_3'^2\int \mathrm{d}\overline{\boldsymbol{k}'}\mathrm{d}\overline{\omega'}C(\boldsymbol{k}',\omega')G(\boldsymbol{k}-\boldsymbol{k}',-\omega+\omega')$$

$$= \mathrm{i}\omega + \lambda(\tau+\boldsymbol{k}^2) - g_3'^2\int \mathrm{d}\overline{\boldsymbol{k}'}\frac{1}{\tau+\boldsymbol{k}'^2}\frac{1}{\mathrm{i}\omega+\lambda\left[2\tau+\boldsymbol{k}'^2+(\boldsymbol{k}-\boldsymbol{k}')^2\right]}, \tag{82}$$

$$\Gamma_{20}(\boldsymbol{k},\omega) = \text{-}\bullet\text{-} + \text{-}\bigcirc\text{-} = -2\lambda - \frac{1}{2}g_3'^2\int \mathrm{d}\overline{\boldsymbol{k}'}\mathrm{d}\overline{\omega'}C(\boldsymbol{k}',\omega')C(\boldsymbol{k}-\boldsymbol{k}',\omega-\omega')$$

$$= -2\lambda - \lambda^3 g_3^2\int \mathrm{d}\overline{\boldsymbol{k}'}\frac{1}{\tau+\boldsymbol{k}'^2}\frac{1}{\tau+(\boldsymbol{k}-\boldsymbol{k}')^2}\frac{2\tau+\boldsymbol{k}'^2+(\boldsymbol{k}-\boldsymbol{k}')^2}{\omega^2+\lambda^2\left[2\tau+\boldsymbol{k}'^2+(\boldsymbol{k}-\boldsymbol{k}')^2\right]^2}, \tag{83}$$

$$\Gamma_{12}(\boldsymbol{k}_1,\omega_1;\boldsymbol{k}_2,\omega_2) = \text{-}\!<\!\text{-} + \text{-}\hexagon\text{-} + \text{-}\hexagon\text{-}$$

$$= g_3' + g_3'^3\int \mathrm{d}\overline{\boldsymbol{k}}\mathrm{d}\overline{\omega}\left[2C(\boldsymbol{k},\omega)G(\boldsymbol{k}_1-\boldsymbol{k},\omega-\omega_1)G(\boldsymbol{k}_2+\boldsymbol{k},\omega+\omega_2) + C(\boldsymbol{k},\omega)G(\boldsymbol{k}_3-\boldsymbol{k},\omega-\omega_3)G(\boldsymbol{k}-\boldsymbol{k}_2,\omega_2-\omega)\right]$$

$$= g_3' + g_3'^3\int \mathrm{d}\overline{\boldsymbol{k}}\frac{1}{\tau+\boldsymbol{k}^2}\left\{\frac{2}{\mathrm{i}\omega_1+\lambda\left[2\tau+\boldsymbol{k}^2+(\boldsymbol{k}_1-\boldsymbol{k})^2\right]}\frac{1}{-\mathrm{i}\omega_2+\lambda\left[2\tau+\boldsymbol{k}^2+(\boldsymbol{k}_2+\boldsymbol{k})^2\right]}\right.$$

$$\left. + \frac{1}{\mathrm{i}\omega_1+\lambda\left[2\tau+(\boldsymbol{k}-\boldsymbol{k}_2)^2+(\boldsymbol{k}_3-\boldsymbol{k})^2\right]}\left[\frac{1}{\mathrm{i}\omega_3+\lambda\left[2\tau+\boldsymbol{k}^2+(\boldsymbol{k}_3-\boldsymbol{k})^2\right]} + \frac{1}{-\mathrm{i}\omega_2+\lambda\left[2\tau+\boldsymbol{k}^2+(\boldsymbol{k}-\boldsymbol{k}_2)^2\right]}\right]\right\}, \tag{84}$$

where the short lines indicate the vertices for clarity and do not enter the expressions of the vertex functions, $\boldsymbol{k}_3 = \boldsymbol{k}_1+\boldsymbol{k}_2$, and $\omega_3 = \omega_1+\omega_2$. One can check that the vertex functions indeed recover their static counterparts when all external frequencies become zero. For example, the integral in Eq. (82) remains unchanged after a replacement $\boldsymbol{k}' \to \boldsymbol{k}-\boldsymbol{k}'$. Adding these two integrals yields

$$\Gamma_{11}(\boldsymbol{k},0) = \lambda(\tau+\boldsymbol{k}^2) - \frac{1}{2}\lambda g_3^2\int \mathrm{d}\overline{\boldsymbol{k}'}\frac{1}{\tau+\boldsymbol{k}'^2}\frac{1}{\tau+(\boldsymbol{k}-\boldsymbol{k}')^2}, \tag{85}$$

which is $\lambda\Gamma_2^{\mathrm{st}}(\boldsymbol{k})$. Similarly, one can show that

$$\Gamma_{12}(\boldsymbol{k}_i,0) = \lambda g_3 + \lambda g_3^3\int \mathrm{d}\overline{\boldsymbol{k}}\frac{1}{\tau+\boldsymbol{k}^2}\frac{1}{\tau+(\boldsymbol{k}_1-\boldsymbol{k})^2}\frac{1}{\tau+(\boldsymbol{k}_2+\boldsymbol{k})^2}, \tag{86}$$

which is simply $\lambda\Gamma_3^{\mathrm{st}}(\boldsymbol{k}_i)$. Moreover, one can also check that the fluctuation-dissipation theorem of Eq. (70) holds to this order, through a similar manipulation.

One effect of the interaction is shifting of the instability point, which is defined by

$$\Gamma_{11}(\boldsymbol{0},0) = 0, \tag{87a}$$
$$\Gamma_{10}(\boldsymbol{0},0) = \lambda h_s, \tag{87b}$$

corresponding to

$$\tau_s = \frac{1}{2}g_3^2\int \mathrm{d}\overline{\boldsymbol{k}}\frac{1}{(\tau_s+\boldsymbol{k}^2)^2}, \tag{88a}$$
$$h_s = \frac{1}{2}g_3\int \mathrm{d}\overline{\boldsymbol{k}}\frac{1}{\tau_s+\boldsymbol{k}^2}, \tag{88b}$$

for a uniform external field H and, hence, uniform h and M. Eqs. (87a) and (88a) determine the point at which the static susceptibility χ diverges (see below). Eqs. (87b) and (88b) specify the field at τ_s for

$$m(\tau_s,h_s) = \langle\varphi(\tau_s,h_s)\rangle = 0. \tag{89}$$

It can be shown explicitly that Eq. (88) is exactly the instability point of the one-loop φ^3 free energy at $m=0$. However, the corresponding ϕ^4 free energy has a vanishingly small barrier, which is in accordance with observations near the spinodal point in non-mean-field systems. Accordingly, this instability point has been advocated as

a new definition of a general spinodal point [24]. As the mean-field spinodal given by Eq. (39) is $\tau_s = 0$, one can replace τ_s in the integrand in Eq. (88a) by its mean-field value in a perturbation expansion. Thus,

$$\tau_s = \frac{1}{2} g_3^2 \int \mathrm{d}\bar{\boldsymbol{k}} \frac{1}{\boldsymbol{k}^4}, \tag{90a}$$

$$h_s = \frac{1}{2} g_3 \int \mathrm{d}\bar{\boldsymbol{k}} \frac{1}{\boldsymbol{k}^2}. \tag{90b}$$

The first and second expressions are infrared divergent for $d \leq 4$ and $d \leq 2$, respectively, because they diverge when $|\boldsymbol{k}| \to 0$ in these dimensions. Note that the momentum integral is cut off at Λ.

The infrared divergences in Eq. (90) affect the position of the instability point, which is a property of a specific system. In fact, these divergences can be subtracted via mass renormalization, which we shall perform shortly. However, similar infrared divergences, which stem from the small momentum behavior at the instability point, persist. In fact, they plague the entire perturbation expansion below an upper critical dimension.

Equation (90a) can be employed in order to express χ as

$$\chi^{-1} = \Gamma_{11}(\boldsymbol{0}, 0)/\lambda = \tau_r \left[1 - \frac{1}{2} g_3^2 \int \mathrm{d}\bar{\boldsymbol{k}} \frac{\tau_r + 2\boldsymbol{k}^2}{(\tau_r + \boldsymbol{k}^2)^2 \boldsymbol{k}^4} \right], \tag{91}$$

as the correction incurred is of higher order in g_3, where $\tau_r = \tau - \tau_s$. Note that the term proportional to τ_r in the integral is equal to zero when $\tau_r = 0$. Therefore, it is again apparent that one can set τ_r in the integrand to its mean-field value if $d > 6$, because the integral is then finite. As a result, χ is again proportional to $\tau_r^{-\gamma}$, with the mean-field result $\gamma = 1$. However, if $d \leq 6$, the integral has an infrared divergence at the instability point and the mean-field result becomes problematic. In fact, in this case, the integral is dominated by small $|\boldsymbol{k}|$'s and, therefore, can be well approximated by

$$\chi^{-1} = \tau_r \left[1 - \frac{\Gamma\left(3 - \frac{d}{2}\right)}{(4\pi)^{d/2}(d-4)} g_3^2 \tau_r^{\frac{d}{2}-3} \right]. \tag{92}$$

This approximation is obtained by extending the momentum cutoff to infinity and using Eqs. (B11), (B2), and (B3), where Γ represents the Euler Gamma function. From Eq. (92), it is apparent that the second term in brackets can become arbitrarily larger than 1 (the first term), for sufficiently small τ_r. Then, the perturbation expansion breaks down. Therefore, this expression identifies the upper critical dimension $d_c = 6$, above which the mean-field theory of the φ^3 model is valid. Accordingly, the spinodal curve and, also, the mean-field spinodal fixed point [48], which build on the mean-field theory, all become valid above d_c, in agreement with previous mean-field analyses [48–50].

Moreover, one can even introduce a Ginzburg effective temperature τ_G to re-express Eq. (92) in the form

$$\chi^{-1} = \tau_r \left[1 - \left(\frac{\tau_r}{\tau_G} \right)^{\frac{d-6}{2}} \right], \tag{93}$$

similar to the critical phenomenon case [68, 69]. Accordingly, for $d > 6$, sufficiently small τ_r (i.e., values sufficiently close to the instability point) can always render the second term in the square brackets smaller than the first, and the mean-field theory is valid. However, for $d < 6$, this statement is only true for $|\tau_r| \gg \tau_G$, which is the Ginzburg criterion [70]. This behavior, therefore, defines an unstable region similar to the critical region within which fluctuations dominate and the mean-field theory fails. Note that, from Eq. (92), this is always true for $d = 4$. Further, this special dimension would have become 2 [70] if the term proportional to τ_r in the integral in Eq. (91) had been neglected.

In what follows (Section 7.2), we show that higher-order corrections also confirm this differentiation of the spatial dimensions. Note that our analysis here is completely parallel to that for the critical phenomena [53, 71, 72]. Therefore, the natural solution to the infrared divergence problem below d_c is the RG theory.

7 Renormalization-group theory

In the previous sections, we have shown that an FOPT can be mapped to the instability point of a φ^3 model, and that the long-wavelength fluctuations near the point result in strong infrared divergences below d_c, which is in close analogy to the critical phenomena. In this section, we shall apply the RG theory in the field-theoretic formulation [51–55, 71, 72] to the φ^3 theory. The RG technique is an effective method for treating both infrared and ultraviolet singularities [54]. The conventional field-theoretic formulation is often concerned with the latter. We shall discuss their relation by applying the usual approach to the present theory and formulate the RG theory for the transition depicted in Fig. 1(c), which is an RG for a massless theory. That is, we consider the RG for the φ^3 theory at the point where Eq. (87a) is satisfied in a similar manner to the critical massless theory.

7.1 Canonical dimensions

To begin, we determine the canonical dimensions of various quantities [53, 72]. These can be obtained via a naïve dimensional analysis, in which $\mathcal{H}$, $\mathcal{H}_3$, and $\mathcal{L}$ are regarded as pure numbers (as they appear in exponentials). All other quantities have the dimension of length, which is taken to be -1, i.e., $[|\boldsymbol{x}|] = -1$, where the square brackets denote the canonical dimension of the quantity

they contain. Therefore, $[|\boldsymbol{k}|] = 1$. Equation (58) then yields $[\lambda t] = -2$ and $[\tau] = 2$, as $\partial/\partial t/\lambda$ and τ play a similar role to ∇^2. Consequently, $[\tilde{\varphi}] = (d+2)/2$ and $[\varphi] = (d-2)/2$ from Eq. (58) and, hence, $[\lambda J] = (d+6)/2$ and $[\lambda\tilde{J}] = (d+2)/2$ from Eq. (21), where the λ factors arise from the time integral. As a result, $[g_3] = (6-d)/2$ and $[h] = [\lambda\tilde{J}] = (d+2)/2$, from Eqs. (17) and (8). Similarly, one finds $[r] = 2$, $[\phi] = (d-2)/2$, $[\tilde{\phi}] = (d+2)/2$, $[H] = (d+2)/2$, and $[g] = 4-d$, for the dynamic ϕ^4 model. Note that $[g_3] = [g] + [M]$, as $[M] = [\phi]$. These dimensions are identical to their static counterparts, as can be readily seen from Eqs. (1) and (8). In addition, from Eq. (59), $[\lambda\varphi(\boldsymbol{k},\omega)] = -(d+6)/2$ and $[\lambda\tilde{\varphi}(\boldsymbol{k},\omega)] = -(d+2)/2$.

Accordingly, one finds from Eqs. (25), (27), and (30) that $[G_{nn'}(\{x_i\})] = n[\phi] + n'[\tilde{\phi}] = (n+n')d/2 + n' - n$ and $[\lambda^{n'+n}\Gamma_{n'n}(\{x_i\})] = n[\lambda J] + n'[\lambda\tilde{J}] = (n+n')d/2 + n' + 3n$. The latter can also be obtained by reattaching the amputated legs of $\Gamma_{n'n}(\{x_i\})$ with integrations and relating it to its corresponding response function. We have used $\{x_i\}$ to represent the set of all the spatial and temporal arguments. Then, from the Fourier transforms defined in Eq. (63) and a similar definition for the vertex function, one obtains $[\lambda^{n+n'}G_{nn'}(\{\boldsymbol{k}_i\},\{\omega_i\})] = [G_{nn'}(\{x_i\})] - (n+n')(d+2) = -(n'+n)d/2 - n' - 3n = n[\lambda\varphi(\boldsymbol{k},\omega)] + n'[\lambda\tilde{\varphi}(\boldsymbol{k},\omega)]$ and $[\Gamma_{n'n}(\{\boldsymbol{k}_i\},\{\omega_i\})] = [\lambda^{n+n'}\Gamma_{n'n}(\{x_i\})] - (n+n')(d+2) = -(n'+n)d/2 + n - n'$. However, the response functions and vertex functions primarily used in Secs. 5 and 6, which are also used below, have an extracted delta function factor of dimension $-d-2$, arising from the global momentum and frequency conservations due to space and time translation invariances, as seen in Eq. (63). Consequently, their dimensions change by this amount and are listed in Table 2. The same symbols are used, but with one power of λ less, for the same reason (i.e., the abovementioned extracted delta function factor).

7.2 Power counting and divergences

We now consider the relation between the infrared and ultraviolet divergences, and show that the consequence of the one-loop analysis in the perturbation expansion conducted above survives to all orders. In particular, the φ^3 theory is non-renormalizable and, thus, the mean-field results are valid for $d > d_c$. However, this theory is super-renormalizable for $d < d_c$, in which the mean-field theory fails and the cubic interaction only is relevant, if a massless theory exists.

We take Eq. (88b) as an example and assume that a mass renormalization has been performed, such that all τ's in the response functions have been replaced with τ_r's, which vanish at the instability point. The integral diverges for $d < 2$, because it behaves as $|\boldsymbol{k}|^{d-2}$ when $\tau_r = 0$, as can be readily seen from Eq. (90b). If we change the variable to $\boldsymbol{k}/\sqrt{\tau_r}$, we obtain

$$h_s = \frac{1}{2} g_3 \tau_r^{d/2-1} \int \mathrm{d}\overline{\boldsymbol{k}} \frac{1}{1+\boldsymbol{k}^2}, \tag{94}$$

where the cutoff now becomes $\Lambda/\sqrt{\tau_r}$. For $d > 2$, the integral is dominated by large $|\boldsymbol{k}|$'s and diverges as $(\Lambda/\sqrt{\tau_r})^{d-2}$. One sees, however, that the τ_r factor simply cancels that outside the integral. In addition, $h_s \sim \Lambda^{d-2}$, a constant, in this case. Therefore, no divergence appears, as appropriate. However, for $d < 2$, the integral is now dominated by small $|\boldsymbol{k}|$'s and can be integrated using Eq. (B1), when $\tau_r \to 0$, yielding

$$h_s = \frac{1}{2(4\pi)^{d/2}} g_3 \Gamma\left(1 - \frac{d}{2}\right) \tau_r^{d/2-1}. \tag{95}$$

This result coincides with that arising from a direct integration of Eq. (88b) for small τ_r and, thus, describes the infrared divergence at the instability point correctly. However, as the new cutoff is now infinity at the instability point, the integral can be directly integrated without the approximated argument that yields Eq. (92). Accordingly, we can study the ultraviolet behavior of large Λ directly in both cases. This enables us to employ the machinery of the field-theoretic RG theory for ultraviolet divergences. From the perspective of statistical physics, this RG procedure separates those universal properties from the microscopic details specified by Λ.

Before extending the analysis to all orders of the perturbation expansion, we first consider the asymptotic dependence of $\Gamma_{n'n}(\{\boldsymbol{k}_i\},\{\omega_i\})$ on Λ in general, i.e., its large momentum behavior. We perform this analysis as an illustration, by considering primitive dependence only and neglecting subintegrations [53, 72]. At the Nth order, a graph of L loops contributing to $\Gamma_{n'n}$ contains the following: L integrations; N vertices, each emitting three lines; $[3N-(n+n')]/2$ internal lines, among which $N-n'$ are response lines each having a $\boldsymbol{k}^{-2}$ factor; and the remaining $(N-n+n')/2$ correlation lines, each having a $\boldsymbol{k}^{-4}$ factor for large $|\boldsymbol{k}|$'s. Consequently, the graph has a total $\boldsymbol{k}$ factor of

$$\begin{aligned}\delta_{n'n} &= L(d+2) - 2(N-n') - 4\times\frac{1}{2}(N-n+n') \\ &= L(d+2) - 4N + 2n,\end{aligned} \tag{96}$$

Table 2 Canonical dimensions.

$\lvert\boldsymbol{x}\rvert$	$\lvert\boldsymbol{k}\rvert$	λt	τ	$\varphi(x)/M$	$\tilde{\varphi}(x)$	g	g_3	$h/[H/(\lambda\tilde{J})]$	λJ	$\lambda\varphi(\boldsymbol{k},\omega)$	$\lambda\tilde{\varphi}(\boldsymbol{k},\omega)$	$\lambda^{n+n'-1}G_{nn'}(\{\boldsymbol{k}_i\},\{\omega_i\})$	$\lambda^{-1}\Gamma_{n'n}(\{\boldsymbol{k}_i\},\{\omega_i\}) \equiv d_{n'n}$
-1	1	-2	2	$\frac{d-2}{2}$	$\frac{d+2}{2}$	$4-d$	$\frac{6-d}{2}$	$\frac{d+2}{2}$	$\frac{d+6}{2}$	$-\frac{d+6}{2}$	$-\frac{d+2}{2}$	$\frac{2-n'-n}{2}d - n' - 3n + 2$	$\frac{2-n'-n}{2}d + n - n' + 2$

powers and is, thus, proportional to $\Lambda^{\delta_{n'n}}$. Note that the frequency integrations are also relevant to the momentum factors, as can be confirmed via Eqs. (81)–(84). The L internal integrations come from the total internal lines less the number of momentum and frequency conservations at each vertex, except for one for the overall conservation, as may be seen in Eq. (63). Therefore,

$$L=\frac{1}{2}[3N-(n+n')]-N+1=\frac{1}{2}(N-n-n')+1. \quad (97)$$

Combining Eqs. (96) and (97), we obtain

$$\begin{aligned}\delta_{n'n}&=\frac{1}{2}(2-n-n')d+n-n'+2+\frac{1}{2}(d-6)N\\&=d_{n'n}-N[g_3],\end{aligned} \quad (98)$$

where we have employed the dimensions of the two quantities given in Table 2. The last expression is intuitive, as the dependence on Λ must come from deducting the contribution from the coupling constant g_3 from the total dimension. All these results may also be checked using Eqs. (81)–(84).

Equation (98) has one overall factor depending only on d and on the n and n' of the vertex function, with the other term depending linearly on both the order of the perturbation expansion and the coupling constant dimension. In fact, as the first factor does not depend on the coupling, it can be shown to correspond to the dimension of the vertex function in the Gaussian theory. Therefore, one concludes that the cutoff-dependence of the vertex functions is independent of the order in the perturbation theory, if the coupling constant is dimensionless. This also applies to the resultant primitive divergences of all the vertex functions when $\Lambda\to\infty$. This finding again identifies a critical dimension $d_c=6$ at which the coupling constant is dimensionless for the φ^3 model considered here. For $d>d_c$, the ultraviolet divergences of the graphs of a vertex function increase in number with the order of the perturbation expansion. As a result, they cannot be absorbed into a finite number of renormalized parameters containing strong Λ or system dependence. In such a case, the theory is then deemed to be non-renormalizable. On the other hand, for $d<d_c$, the degree of the primitive divergences decreases as one goes to higher orders in the perturbation theory. The theory is then deemed super-renormalizable, while a theory with $d=d_c$ is renormalizable [53, 71, 72].

We now relate this asymptotic dependence to the infrared behavior of the graph, which contributes $D_{n'n}$ to $\Gamma_{n'n}$. For simplicity, let us set all its external momenta and frequencies to zero and change its integration variables again, such that

$$\boldsymbol{k}'=\boldsymbol{k}/\sqrt{\tau_r},\quad \omega'=\omega/\tau_r. \quad (99)$$

As a result,

$$D_{n'n}=\tau_r^{\delta_{n'n}/2}D'_{n'n}. \quad (100)$$

The remaining integral in $D'_{n'n}$ has no infrared divergences at $\tau_r\to 0$, as can be seen from Eq. (94). However, when $d>d_c$, i.e., the interaction is non-renormalizable, $D'_{n'n}$ has ultraviolet divergences proportional to $(\Lambda/\sqrt{\tau_r})^{\delta_{n'n}}$ for sufficiently high orders in the perturbation expansion. Yet, similar to our example, the two factors of τ_r cancel exactly, leaving only finite numbers in every order of the perturbation. As a result, the mean-field behavior survives. For those vertex functions with large n' and n (for $d>2$), there may exist some lower-order diagrams having $\delta_{n'n}<0$ (from Eq. (98)), which are, thus, ultraviolet convergent. As $\delta_{n'n}$ increases with order N, the leading infrared divergence comes from the lowest one-loop term with only vertices having the smallest $d_{n'n}$ [53].

On the other hand, when $d<d_c$, the theory is super-renormalizable and only a finite number of diagrams have ultraviolet divergences. These divergences can then be incorporated into a redefinition of the model parameters such that the theory built on these redefined parameters converges at large momenta. This means that the large-scale behavior of the theory does not depend on its microscopic details as prescribed by Λ and, thus, universality ensues.

Note that, for $d<d_c$ and excluding those ultraviolet divergent diagrams, the other diagrams are superficially convergent via power counting and the infrared divergences are, thus, given by $\tau_r^{\delta_{n'n}/2}$, or may be even more singular when $\tau_r\to 0$. Moreover, as shown by Eq. (98), these singularities increase without bound with the order of perturbation. However, we now demonstrate that the most infrared-divergent terms in the perturbation theory are described order by order by the φ^3 theory [53, 71, 72]. All higher-order couplings are irrelevant as far as the infrared behavior is concerned.

Consider, for example, a theory containing ι types of interaction vertices, each emitting one $\tilde{\varphi}$ line and $n_\iota-1$ φ lines. For such a theory, Eqs. (96) and (97) become

$$\delta'_{n'n}=L'(d+2)-2\sum_\iota N_\iota n_\iota+2N+2n, \quad (101)$$

$$L'=\frac{1}{2}\left[\sum_\iota N_\iota n_\iota-(n+n')\right]-N+1, \quad (102)$$

and, therefore,

$$\begin{aligned}\delta'_{n'n}&=\frac{1}{2}(2-n-n')d+n-n'+2\\&\quad+\sum_\iota N_\iota\left(\frac{1}{2}n_\iota d-n_\iota-d\right)\\&=d_{n'n}-\sum_\iota N_\iota[g_\iota],\end{aligned} \quad (103)$$

where $N=\sum_\iota N_\iota$ and $[g_\iota]=-n_\iota(d-2)/2+d$ is the dimension of the coupling constant with n_ι fields

with $g_4 \equiv g$. One now sees that $-[g_\iota]$ increases with n_ι for $d > 2$. Thus, the minimum n_ι gives minimum $n_\iota(d-2)/2 - d$ and, hence, minimum $\delta'_{n'n}$. This is the most negative value and, therefore, it characterizes the most infrared-divergent diagrams for each perturbation expansion order. In the case of the critical phenomena of the Ising model, the order parameter has an inversion symmetry. Thus, the smallest n_ι is 4, and the ϕ^4 model reproduces the sum of the most infrared-divergent contributions order-by-order in a mean-field expansion below its critical dimension of $d_c = 2n_\iota/(n_\iota - 2) = 4$, at which $[g_\iota] = 0$ [53, 71]. In systems with FOPTs, as their symmetries have already been broken, the smallest n_ι is 3. Thus, all other terms (including terms with more spatial derivatives, which induce $\boldsymbol{k}$ factors in the numerators of the momentum integrals) are infrared irrelevant for $d < 6$. At $d = 6$, the mean-field behavior is modified by logarithmic corrections, as in the critical phenomenon case.

7.3 RG scheme and renormalization constants

For $d < 6$, we have seen that the infrared singularities at the instability points of an FOPT can be described by a φ^3 theory. In these dimensions, the ultraviolet divergences of the theory are super-renormalizable and can, thus, be absorbed in a few parameters by renormalization. There are usually two perturbation RG schemes that can handle these divergences. One uses the $\varepsilon = 6-d$ expansion and the other works directly in a fixed dimension. We adopt the first scheme and study the massless theory only, as mentioned above. We take this approach because we have been focusing on the FOPT described by Fig. 1(c). Although the massless theory has problems associated with infrared divergences and cannot yield results such as universal amplitude ratios [73–78], it can nevertheless give the exponents with which we are concerned here. We apply the technique of dimensional regulation to the ultraviolet divergent integrals and utilize the minimal RG method to subtract the resultant dimensional poles only [79]. In fact, this technique involving analytical continuation in the number of spatial dimensions and the pushing of Λ to infinity has been argued to be a more natural approach to the critical phenomena and, similarly, to the "unstable" phenomena here. The reasoning behind this is that one can then focus on the infrared behavior alone, without resorting to the ultraviolet divergences in a theory with a finite cutoff [62]. The RG method of minimal subtraction has an additional advantage of decoupling the dynamics from the statics without the need for a deliberate choice of renormalization conditions [60]. As a result, the static renormalization factors can be chosen to be identical to those of the corresponding equilibrium model. This feature can be used as a self-check and can also simplify the manipulations.

As we use the ε expansion, we renormalize the theory at $d_c = 6$. The first task is to identify those vertex functions that are superficially divergent. These functions are given by $\delta_{n'n} \geq 0$ at d_c, which, at this dimension, is simply the $d_{n'n}$ of the pertinent vertex functions. From Table 2, we find that these vertex functions are Γ_{10}, which is quartic divergent, Γ_{11}, which is quadratic divergent, and Γ_{20} and Γ_{12}, both of which are logarithmic divergent. Therefore, we should, in principle, introduce four renormalization constants to absorb the divergences. However, they are not all independent: Γ_{20} is related to Γ_{11}, by Eq. (70). Consequently, we are required to introduce three renormalization constants only. Of course, we must perform subtractions or mass renormalizations to handle the quadratic and quartic divergences of Γ_{10} and Γ_{11}. However, as we shall study the massless theory and utilize the dimensional regulation technique, these subtractions become zero, because massless integrals such as Eq. (90) are zero in the dimensional regulation. This does not mean, of course, that the instability point is not shifted. Note that we do not consider composite operators and the free energy here.

Although we plan to work with the massless theory, we consider an external field that drives the transition, as shown in Fig. 1(c). Accordingly, we rewrite our relevant action as

$$\mathcal{L} = \int \mathrm{d}\boldsymbol{x}\mathrm{d}t\tilde{\varphi}\left[\frac{\mathrm{d}\varphi}{\mathrm{d}t} - \lambda\left(\nabla^2\varphi - \frac{1}{2}g_3\varphi^2 + h + \tilde{\varphi}\right)\right], \tag{104}$$

for which we have neglected τ_s and h_s, as they are zero in the dimensional regulation. The renormalizability of this massless theory for $d \leq 6$ means that, by choosing the renormalization factors $Z(u_R, \varepsilon)$ to be

$$\begin{aligned} &\varphi = Z_\varphi^{1/2}\varphi_R, \quad \tilde{\varphi} = Z_{\tilde{\varphi}}^{1/2}\tilde{\varphi}_R, \quad \lambda = Z_\lambda\lambda_R, \\ &u = Z_u u_R, \quad u = g_3 N_d^{1/2}\mu^{-\varepsilon/2}, \end{aligned} \tag{105}$$

the renormalized $G_{nn'R}$ and $\Gamma_{n'nR}$ are finite at every order in an expansion in u_R as $\varepsilon \to 0$, where μ is an arbitrary momentum scale, N_d is given by Eq. (B2), and the subscript R' s denote renormalized quantities. Note that the renormalized $G_{nn'R}$ and $\Gamma_{n'nR}$ are functions of the renormalized parameters λ_R and u_R satisfying

$$G^c_{nn'} = Z_\varphi^{n/2} Z_{\tilde{\varphi}}^{n'/2} G_{nn'R}, \tag{106}$$

$$\Gamma_{n'n} = Z_{\tilde{\varphi}}^{-n'/2} Z_\varphi^{-n/2} \Gamma_{n'nR}, \tag{107}$$

from their definitions. As the fluctuation-dissipation theorem must hold in both the unrenormalized and renormalized forms, from Eqs. (70), (105), and (107), we find

$$Z_\lambda = Z_\varphi^{1/2} Z_{\tilde{\varphi}}^{-1/2}. \tag{108}$$

This confirms that only three Z's are required.

We now compute these factors to one-loop order using the method of minimal subtraction and show that they indeed render the vertex functions finite.

Firstly, we choose Eq. (85) to fixed Z_φ. Note that, in the following sections, all τ must be set to zero when referring to the equations in Section 6, as we are considering a massless theory. Using Eq. (B12) and noting that $\Gamma(2-d/2)$ contributes an ε pole from Eq. (B4) (hence, the other Γ functions can be evaluated directly at $d=6$), we find

$$\Gamma_{11}(\boldsymbol{k},0)=\lambda\boldsymbol{k}^2+\frac{1}{6\varepsilon}\lambda g_3^2 N_d\left(\boldsymbol{k}^2\right)^{\frac{d}{2}-2}\left[1+O(\varepsilon)\right]. \quad (109)$$

As mentioned in Section 6, $\Gamma_{11}(\boldsymbol{k},0)=\lambda\Gamma_2^{\rm st}(\boldsymbol{k})$. Therefore, using the definition of u in Eq. (105), we obtain

$$\Gamma_2^{\rm st}(\boldsymbol{k})=\boldsymbol{k}^2\left\{1+\frac{1}{6\varepsilon}u^2\left[1+O(\varepsilon)\right]\right\}, \quad (110)$$

where we have expanded $(|\boldsymbol{k}|/\mu)^{-\varepsilon}=1-\varepsilon\ln(|\boldsymbol{k}|/\mu)+O(\varepsilon^2)$ and neglected all the terms that add to order $O(\varepsilon)$ in Eq. (110) consistently. It is apparent that the neglected $\ln(|\boldsymbol{k}|/\mu)$ can never overpower the overall $\boldsymbol{k}^2$ factored out in Eq. (110) in the infrared limit; thus, we obtain a renormalized massless theory for every order in u, such that $\Gamma_{11}(\boldsymbol{0},0)=0$. It is also apparent that the residue of the pole is independent of the external momentum. In fact, this is a general feature by which the residue of the pole of highest order in a graph must be independent of the external momenta. Further, the momentum dependence of the poles of lower order must be canceled for any set of external momenta [72]. These features offer a check on the calculations.

According to Eq. (107), one can choose Z_φ in the method of minimal subtraction to subtract the pole in Eq. (110) only, such that

$$\Gamma_{2R}^{\rm st}(\boldsymbol{k},\mu)=Z_\varphi\Gamma_2^{\rm st}(\boldsymbol{k}) \quad (111)$$

is finite. This yields

$$Z_\varphi=1-\frac{1}{6\varepsilon}u^2. \quad (112)$$

Next, we choose Eq. (82) with $\boldsymbol{k}=\boldsymbol{0}$, to fix $Z_{\tilde\varphi}$. Using Eq. (B11) formally and factoring out the ε pole, we find

$$\begin{aligned}\Gamma_{11}(\boldsymbol{0},\omega)&=\mathrm{i}\omega+\frac{1}{2\varepsilon}\lambda g_3^2 N_d\left(\frac{\mathrm{i}\omega}{2\lambda}\right)^{\frac{d}{2}-2}\left[1+O(\varepsilon^2)\right],\\&=\mathrm{i}\omega\left\{1+\frac{1}{4\varepsilon}u^2\left[1+O(\varepsilon)\right]\right\},\end{aligned} \quad (113)$$

where the definition of u in Eq. (105) has been used and powers of $\ln[\mathrm{i}\omega/(2\lambda\mu^2)]$ have also been neglected. Similar features to the previous case can be observed here.

Following Eq. (107), we then choose

$$(Z_\varphi Z_{\tilde\varphi})^{1/2}=1-\frac{1}{4\varepsilon}u^2, \quad (114)$$

so as to subtract the pole in Eq. (113) and obtain

$$Z_{\tilde\varphi}=1-\frac{1}{3\varepsilon}u^2, \quad (115)$$

using Eq. (112).

Equation (115) can be checked using the usual method, employing

$$\begin{aligned}\left.\frac{\partial\Gamma_{11}(\boldsymbol{k},\omega)}{\partial(\mathrm{i}\omega)}\right|_{\omega=0}&=1+g_3^2 I_1(\boldsymbol{k})\\&=1+\frac{1}{4\varepsilon}u^2\left[\frac{|\boldsymbol{k}|}{\mu}\right]^{-\varepsilon}\left[1+O(\varepsilon)\right],\end{aligned} \quad (116)$$

from Eqs. (B13) and (B21). This again yields Eqs. (114) and (115). We can also use

$$\begin{aligned}\Gamma_{20}(\boldsymbol{k},0)&=-2\lambda-\lambda g_3^2 I_2(\boldsymbol{k})\\&=-2\lambda\left\{1+\frac{1}{4\varepsilon}u^2\left[\frac{|\boldsymbol{k}|}{\mu}\right]^{-\varepsilon}\left[1+O(\varepsilon)\right]\right\},\end{aligned} \quad (117)$$

directly, from Eqs. (B14) and (B22). Therefore, Eq. (107) gives

$$\begin{aligned}\Gamma_{20R}(\boldsymbol{k},0,\mu)&=Z_{\tilde\varphi}\Gamma_{20}(\boldsymbol{k},0)\\&=-2\lambda_R Z_\lambda Z_{\tilde\varphi}\left\{1+\frac{1}{4\varepsilon}u^2\left[1+O(\varepsilon)\right]\right\},\end{aligned} \quad (118)$$

with the aid of Eq. (105). Therefore, we obtain

$$Z_\lambda Z_{\tilde\varphi}=1-\frac{1}{4\varepsilon}u^2=(Z_\varphi Z_{\tilde\varphi})^{1/2}, \quad (119)$$

which recovers Eq. (108), as appropriate. Of course, because Eq. (108) is true, Eq. (119) again consistently yields Eq. (115) using Eq. (112).

Finally, we utilize Eq. (86) to determine Z_u. We obtain

$$\begin{aligned}\Gamma_{3R}^{\rm st}(\boldsymbol{k},\mu)&=\Gamma_{12R}(\boldsymbol{k},0,\mu)/\lambda_R\\&=Z_\varphi^{3/2}\Gamma_{12R}(\boldsymbol{k},0,\mu)/\lambda_R\\&=Z_\varphi^{3/2}\left[g_3+g_3^3 I_3(\boldsymbol{k}_1,\boldsymbol{k}_2)\right]\\&=Z_\varphi^{3/2}Z_u u_R N_d^{-1/2}\mu^{\varepsilon/2}\left\{1+\frac{1}{\varepsilon}u^2\left[1+O(\varepsilon)\right]\right\},\end{aligned} \quad (120)$$

from Eqs. (107), (B15), (B23), and (105). Therefore,

$$Z_\varphi^{3/2}Z_u=1-\frac{1}{\varepsilon}u^2, \quad (121)$$

which yields

$$Z_u=1-\frac{3}{4\varepsilon}u^2, \quad (122)$$

using Eq. (112).

However, all the Z factors must be a series in u_R instead of u itself. Using Eqs. (105) and (122), we obtain

$$u = Z_u u_R = u_R - \frac{3}{4\varepsilon}u_R^3, \tag{123}$$

through iteration. Therefore, to one-loop order, all u^2 can simply be replaced by u_R^2. Finally, we have

$$Z_\varphi = 1 - \frac{1}{6\varepsilon}u_R^2, \quad Z_{\tilde\varphi} = 1 - \frac{1}{3\varepsilon}u_R^2, \quad Z_u = 1 - \frac{3}{4\varepsilon}u_R^2, \tag{124}$$

from Eqs. (112), (115), and (122).

7.4 Renormalized massless theory

We have obtained a finite renormalized massless theory by incorporating the dimensional poles into the three Z factors. We can then, in principle, determine the unstable properties using this theory. For example, one can use Eq. (85) to find the instability exponent η, which is simply defined as $\Gamma(\boldsymbol{k},0) \to |\boldsymbol{k}|^{2-\eta}$ for small $|\boldsymbol{k}|$ at the instability point, as can be seen from Eq. (76). Indeed, using Eqs. (107), (105), (124), and (B21), we find that, to one-loop order, Eq. (109) becomes

$$\begin{aligned}
&\Gamma_{11R}(\boldsymbol{k},0,\mu) = (Z_\varphi Z_{\tilde\varphi})^{1/2}\Gamma_{11}(\boldsymbol{k},0)\\
&= Z_\varphi\lambda_R\boldsymbol{k}^2\left\{1 + \frac{1}{6\varepsilon}g_3^2 N_d|\boldsymbol{k}|^{-\varepsilon}\left[1 + \frac{7}{12}\varepsilon + O(\varepsilon^2)\right]\right\}\\
&= \lambda_R\left(1 + \frac{7}{72}u_R^2\right)\boldsymbol{k}^2\left[1 - \frac{1}{6}u_R^2\ln\frac{|\boldsymbol{k}|}{\mu} + O(u_R^4)\right]\\
&\to \lambda_R\left[1 + \frac{7}{72}u_R^2 + O(u_R^4)\right]\boldsymbol{k}^{2-\eta}
\end{aligned} \tag{125}$$

with

$$\eta = \frac{1}{6}u_R^2, \tag{126}$$

for small μ's in equivalence to small momenta, if one replaces $\boldsymbol{k}$ with $\mu\boldsymbol{k}$. In Eq. (125), the first line is an example of Eq. (107) and the second agrees with Eq. (111), for the static vertex function. Accordingly, it is clearly apparent that the result of the fluctuation-dissipation theorem, Eq. (108), in fact ensures the correct static limit at $\omega = 0$. The third line in Eq. (125) exhibits no poles correctly, as they simple cancel among themselves. Note that we have factored out a non-divergent part here and exponentiated the terms in the braces in the last line. The manipulation has a somewhat "brute force" appearance at this order, but it shall be supported by the RG analysis.

Similarly, one finds from Eqs. (113) and (76) that

$$\begin{aligned}
\Gamma_{11R}(\boldsymbol{0},\omega,\mu) &= \mathrm{i}\omega\left[1 - \frac{1}{8}u_R^2\ln\frac{\mathrm{i}\omega}{2\lambda_R\mu^2} + O(u_R^3)\right]\\
&\to \mathrm{i}\lambda_R\left[1 - \frac{1}{8}u_R^2\ln 2 + O(u_R^3)\right]\left(\frac{\omega}{\lambda_R}\right)^{\frac{2-\eta}{z}}.
\end{aligned} \tag{127}$$

Hence, we obtain

$$z = 2 - \eta + \frac{1}{4}u_R^2 = 2 + \frac{1}{12}u_R^2 \tag{128}$$

to one-loop order in the small-μ limit.

These results indicate that we should examine whether or not a fixed u_R^* independent of μ exists in the small-μ limit. If u_R^* is zero, we recover the mean-field result. However, if there is a finite u_R^* when $\mu \to 0$, we obtain finite η and z, which are independent of the scale μ and are, thus, universal.

7.5 RG equations

In the massless theory, we introduce μ as a substitute for the natural mass scale in order to define the dimensionless coupling constant u. Different values of μ yield different renormalized vertex functions. However, they are physically equivalent, as they are related to each other by a finite multiplicative renormalization transformation [53, 54, 72]. This can be easily seen from Eq. (107). The renormalized vertex functions at different μ's are multiplicatively related to the unrenormalized functions of the same given bare theory. Therefore, they are also multiplicatively related by transformation factors that must be finite, because the renormalized functions they relate are finite. All such transformations form an RG. The infinitesimal transformations in the case of the massless theory satisfy a differential RG equation. Further, this equation yields useful results such as scaling and universality, which lie beyond the perturbation theory.

We now construct the RG equation. We first consider the case in which $h = 0$, i.e., exactly at the instability point. As the bare functions are independent of μ, we derive the RG equation for the renormalized $\Gamma_{n'nR}$ as

$$\left(\mu\frac{\partial}{\partial\mu} + \gamma_\lambda\lambda_R\frac{\partial}{\partial\lambda_R} + \beta\frac{\partial}{\partial u_R} - \frac{1}{2}n\gamma_\varphi - \frac{1}{2}n'\gamma_{\tilde\varphi}\right)\Gamma_{n'nR} = 0, \tag{129}$$

by differentiating Eq. (107), where all quantities are renormalized and, therefore, finite. In Eq. (129), the Wilson functions are defined as derivatives at constant bare parameters (φ, $\tilde\varphi$, λ, g_3), i.e.,

$$\begin{aligned}
\gamma_\lambda(u_R) &= \mu\frac{\partial\ln\lambda_R}{\partial\mu}, \quad \beta(u_R) = \mu\frac{\partial u_R}{\partial\mu},\\
\gamma_\varphi(u_R) &= \mu\frac{\partial\ln Z_\varphi}{\partial\mu}, \quad \gamma_{\tilde\varphi}(u_R) = \mu\frac{\partial\ln Z_{\tilde\varphi}}{\partial\mu}.
\end{aligned} \tag{130}$$

Taking logarithms followed by partial derivatives of the equations associated with λ and u in Eq. (105) at the constant bare parameters, and taking Eq. (108) into account, we find

$$\gamma_\lambda = -\mu\frac{\partial \ln Z_\lambda}{\partial \mu} = \frac{1}{2}\gamma_{\tilde{\varphi}} - \frac{1}{2}\gamma_\varphi, \tag{131}$$

$$\begin{aligned}\beta(u_R) &= -\frac{1}{2}\varepsilon u_R - \mu\frac{\partial \ln Z_u}{\partial \mu}u_R \\ &\equiv -\frac{1}{2}\varepsilon u_R - \gamma_u u_R.\end{aligned} \tag{132}$$

Next, we consider the case in which a uniform external field $H_R \neq h_s + rM + gM^3/6$, from Eq. (6), i.e., h_R is not exactly at h_s. In this case, m is not zero. Therefore, Eq. (87b) becomes

$$\lambda_R h_R(\omega) = \Gamma_{10R}(\mathbf{0}, 0; m_R(\omega)). \tag{133}$$

We have included the case in which m_R depends on time. Expanding the right hand side at the instability point at which $m(\tau_s, h_s) = 0$ and Eq. (87b) holds, we obtain

$$\lambda_R h_R(\omega, \lambda_R, m_R, u_R, \mu) = \sum_{n=1}^{\infty}\frac{1}{n!}\Gamma_{1nR}(\mathbf{0}, 0; 0)m_R^n. \tag{134}$$

Therefore, using Eq. (129) and noting that $m = Z_\varphi^{1/2}m_R$, similar to φ, we find

$$\left(\mu\frac{\partial}{\partial\mu} + \gamma_\lambda\lambda_R\frac{\partial}{\partial\lambda_R} + \beta\frac{\partial}{\partial u_R} - \frac{1}{2}\gamma_\varphi m_R\frac{\partial}{\partial m_R} - \frac{1}{2}\gamma_\varphi\right)h_R = 0. \tag{135}$$

This derivation can also be directly verified by substituting Eq. (133) into this expression.

Another method to derive Eq. (135) is to note that Eq. (133) can also be written in bare form with a bare field h. Using Eqs. (105) and (107), the transformation of this term is then found to be

$$h = Z_\varphi^{-1/2}h_R, \tag{136}$$

which assures $\lambda h\tilde{\varphi} = \lambda_R h_R\tilde{\varphi}_R$. Therefore, $\lambda_R h_R$ is only a shift of the source $\tilde{J}$. Equation (136) is identical to its static form. Taking this for granted and using Eq. (107) for Γ_{10}, we again obtain Eq. (108). Differentiating Eq. (136) with respect to μ then yields Eq. (135) directly.

7.6 Solutions to RG equations, fixed points, and instability exponents

Equations (129) and (135) can be solved via the method of characteristics [53, 72]. First, we consider the first equation. Along a characteristic parameterized by κ and determined by flow equations and their respective initial conditions:

$$\kappa\frac{\mathrm{d}\mu(\kappa)}{\mathrm{d}\kappa} = \mu, \quad \mu(1) = \mu, \tag{137a}$$

$$\kappa\frac{\mathrm{d}\lambda_R}{\mathrm{d}\kappa} = \gamma_\lambda\lambda_R(\kappa), \quad \lambda_R(1) = \lambda_R, \tag{137b}$$

$$\kappa\frac{\mathrm{d}u_R(\kappa)}{\mathrm{d}\kappa} = \beta[u_R(\kappa)], \quad u_R(1) = u_R, \tag{137c}$$

$\Gamma_{n'n}$ satisfies

$$\kappa\frac{\mathrm{d}\Gamma_{n'nR}}{d\kappa} = \left(\frac{1}{2}n\gamma_\varphi + \frac{1}{2}n'\gamma_{\tilde{\varphi}}\right)\Gamma_{n'nR}. \tag{138}$$

The solution of this equation is

$$\Gamma_{n'nR}(\{\boldsymbol{k}_i\}, \{\omega_i\}; \lambda_R(\kappa), u_R(\kappa), \mu\kappa) = \Gamma_{n'nR}(\{\boldsymbol{k}_i\}, \{\omega_i\}; \lambda_R, u_R, \mu)\exp\left\{\frac{1}{2}\int_1^\kappa\frac{\mathrm{d}x}{x}\left[n\gamma_\varphi(x) + n'\gamma_{\tilde{\varphi}}(x)\right]\right\}, \tag{139}$$

where we have used the solution of Eq. (137a), $\mu(\kappa) = \mu\kappa$.
On the other hand, from the naïve dimensional analysis conducted in Section 7.1, we have a generalized homogeneous relation

$$\Gamma_{n'nR}(\{\boldsymbol{k}_i\}, \{\omega_i\}; \lambda_R, u_R, \mu) = \kappa^{d_{n'n}}\lambda_R\Gamma_{n'nR}(\{\boldsymbol{k}_i/\kappa\}, \{\omega_i/(\lambda_R\kappa^2)\}; u_R, \mu/\kappa). \tag{140}$$

Note the λ_R factor from Table 2, for dimensional reasons. Applying this equation to the left hand side of Eq. (139), we find

$$\Gamma_{n'nR}(\{\kappa\boldsymbol{k}_i\}, \{\omega_i\}; \lambda_R, u_R, \mu) = \lambda_R(\kappa)\Gamma_{n'nR}(\{\boldsymbol{k}_i\}, \{\omega_i/(\lambda_R(\kappa)\kappa^2)\}; u_R(\kappa), \mu)\kappa^{d_{n'n}}\exp\left(-\frac{1}{2}\int_1^\kappa\frac{\mathrm{d}x}{x}\left(n\gamma_\varphi + n'\gamma_{\tilde{\varphi}}\right)\right), \tag{141}$$

where we have relabeled $\boldsymbol{k}$ with $\kappa\boldsymbol{k}$. The μ dependence here is completely free and can be suppressed. In fact, one can simply set $\kappa = \mu$ and set μ itself (the value at $\kappa = 1$) to simply 1 initially.

Equation (141) relates the vertex functions at different wavenumbers. In particular, it quantifies the manner in

which the vertex functions change when the wavenumbers are reduced. No simple scaling occurs, however, as the momenta are rescaled. The reverse occurs when the coupling constant reaches a value such that any further rescaling does not affect it. This value is found at the fixed points satisfying

$$\beta(u_R^*) = 0. \tag{142}$$

At such a fixed point, u_R does not change with κ from Eq. (137c). As they depend on κ through u_R, γ_φ, $\gamma_{\bar{\varphi}}$, and γ_λ also assume their fixed-point values, which are all marked by stars below. As a result, Eq. (137b) yields

$$\lambda_R(\kappa) = \lambda_R \kappa^{\gamma_\lambda^*}, \tag{143}$$

and, using Eq. (131) for γ_λ, Eq. (141) becomes

$$\varGamma_{n'nR}(\{\kappa \boldsymbol{k}_i\}, \{\omega_i\}; \lambda_R, u_R^*) = \lambda_R \varGamma_{n'nR}(\{\boldsymbol{k}_i\}, \{\omega_i/\lambda_R\}\kappa^{-2-\gamma_\lambda^*}; u_R^*)\kappa^{d_{n'n} - \frac{1}{2}(n+1)\gamma_\varphi^* - \frac{1}{2}(n'-1)\gamma_{\bar{\varphi}}^*}, \tag{144}$$

which exhibits exact scaling. In particular,

$$\varGamma_{11R}(\kappa \boldsymbol{k}, \omega; \lambda_R, u_R^*) = \lambda_R \varGamma_{11R}(\boldsymbol{k}, (\omega/\lambda_R)\kappa^{-2-\gamma_\lambda^*}; u_R^*)\kappa^{2-\gamma_\varphi^*}, \tag{145}$$

using Table 2 for $d_{n'n}$. Compared with Eq. (76), we find that

$$z = 2 + \gamma_\lambda^* = 2 + \frac{1}{2}\gamma_{\bar{\varphi}}^* - \frac{1}{2}\gamma_\varphi^*, \tag{146a}$$

$$\eta = \gamma_\varphi^*, \tag{146b}$$

$$\gamma_{\bar{\varphi}}^* = \eta + 2z - 4, \tag{146c}$$

using Eq. (131). Therefore, Eq. (145) becomes

$$\varGamma_{11R}(\kappa \boldsymbol{k}, \omega; \lambda_R, u_R^*) = \lambda_R \varGamma_{11R}(\boldsymbol{k}, (\omega/\lambda_R)\kappa^{-z}; u_R^*)\kappa^{2-\eta}. \tag{147}$$

For $\omega = 0$, $\boldsymbol{k} = \boldsymbol{1}$, and $\kappa = |\boldsymbol{k}|$, Eq. (147) reads

$$\varGamma_{11R}(\boldsymbol{k}, 0; \lambda_R, u_R^*) = \lambda_R \varGamma_{11R}(\boldsymbol{1}, 0; u_R^*)|\boldsymbol{k}|^{2-\eta}, \tag{148}$$

which is, in fact, Eq. (125). For $\boldsymbol{k} = \boldsymbol{0}$ and $\kappa = (\omega/\lambda_R)^{1/z}$, Eq. (147) becomes

$$\varGamma_{11R}(\boldsymbol{0}, \omega; \lambda_R, u_R^*) = \lambda_R \varGamma_{11R}(\boldsymbol{0}, 1; u_R^*)(\omega/\lambda_R)^{(2-\eta)/z}, \tag{149}$$

which can be shown to be simply Eq. (127). Accordingly, we obtain

$$\varGamma_{11R}(\boldsymbol{k}, 0; \lambda_R, u_R^*) = \lambda_R \left(1 - \frac{7}{108}\varepsilon\right)|\boldsymbol{k}|^{2+\frac{\varepsilon}{9}}, \tag{150}$$

$$\varGamma_{11R}(\boldsymbol{0}, \omega; \lambda_R, u_R^*) = \mathrm{i}\lambda_R \left(1 + \frac{1}{12}\varepsilon\right)\left(\frac{\omega}{\lambda_R}\right)^{1+\frac{\varepsilon}{12}}, \tag{151}$$

to one-loop order, using Eqs. (165) and (166) below.

Similarly, defining one additional flow equation associated with m_R as

$$\kappa \frac{\mathrm{d}m_R(\kappa)}{\mathrm{d}\kappa} = -\frac{1}{2}\gamma_\varphi m_R, \quad m_R(1) = m_R, \tag{152}$$

we arrive at the counterpart of Eq. (141), which is expressed as

$$h_R(t, \lambda_R, m_R, u_R) = \kappa^{(d+2)/2} \exp\left(-\frac{1}{2}\int_1^\kappa \frac{\mathrm{d}x}{x}\gamma_\varphi\right) \times h_R(\lambda_R(\kappa)t\kappa^2, m_R(\kappa)\kappa^{-(d-2)/2}, u_R(\kappa)), \tag{153}$$

where we have switched to the time domain and used Table 2. At the fixed point,

$$m_R(\kappa) = m_R \kappa^{-\frac{1}{2}\eta}, \tag{154}$$

from Eq. (152) and, hence,

$$h_R(t, \lambda_R, m_R, u_R^*) = \kappa^{\beta\delta/\nu} h_R(\lambda_R t\kappa^z, m_R\kappa^{-\beta/\nu}, u_R^*), \tag{155}$$

with

$$\beta\delta/\nu = \frac{1}{2}(d + 2 - \eta), \tag{156}$$

$$\beta/\nu = \frac{1}{2}(d - 2 + \eta), \tag{157}$$

$$\delta = \frac{d + 2 - \eta}{d - 2 + \eta}, \tag{158}$$

using Eqs. (143) and (146). Choosing $\kappa \sim m_R^{\nu/\beta}$ in Eq. (155) yields a scaling form for the equation of state at the instability point

$$h_R(t, \lambda_R, m_R) = m_R^\delta f_3(\lambda_R t m_R^{\nu z/\beta}), \tag{159}$$

where f_3 is a scaling function.

We have solved the RG equations and studied the behavior of a system for which the renormalized coupling constant lies exactly at the fixed point. We now investigate how and when the renormalized coupling constant flows into the fixed point.

Expanding $\beta(u_R)$ in the vicinity of a simple fixed point u_R^*, such that

$$\beta(u_R) = \beta'(u_R - u_R^*), \tag{160}$$

we find, from Eq. (137c),

$$u_R(\kappa) - u_R^* = (u_R - u_R^*)\kappa^{\beta'}, \tag{161}$$

where β' is the derivative of β at u_R^*. It is, therefore, apparent that, if $\beta' > 0$, $u_R(\kappa)$ flows to u_R^* for $\kappa \to 0$ independent of the initial renormalized coupling constant.

On the other hand, if $\beta' < 0$, $u_R(\kappa)$ flows to u_R^* for $\kappa \to \infty$ for an arbitrary initial renormalized coupling constant near the fixed point. We label the fixed point in the first case as "infrared stable" and that in the second case as "ultraviolet stable." The reasoning behind this is that smaller and smaller momenta and, thus, the large-scale behavior, are probed as $\kappa \to 0$, as indicated by Eq. (144).

We have computed all necessary Z's in Eq. (124) to one-loop order. Accordingly, Eqs. (130) and (132) yield

$$\beta(u_R) = -\frac{1}{2}\varepsilon u_R - \frac{3}{4}u_R^3, \tag{162}$$

$$\gamma_\varphi = \beta(u_R)\frac{\partial \ln Z_\varphi}{\partial u_R} = \frac{1}{6}u_R^2, \tag{163}$$

$$\gamma_{\tilde\varphi} = \beta(u_R)\frac{\partial \ln Z_{\tilde\varphi}}{\partial u_R} = \frac{1}{3}u_R^2. \tag{164}$$

Equation (162) has three fixed points. The Gaussian fixed point $u_R^* = 0$ is infrared stable for $\varepsilon < 0$ or $d > 6$ and ultraviolet stable for $\varepsilon > 0$. The other two purely imaginary conjugate fixed points are

$$u_R^{*2} = -\frac{2}{3}\varepsilon. \tag{165}$$

Although these are imaginary values, they are infrared stable and, thus, control the large-scale behavior for $\varepsilon > 0$ or $d < 6$. Moreover, at these imaginary fixed points,

$$\eta = -\frac{1}{9}\varepsilon, \quad z = 2 - \frac{1}{18}\varepsilon, \quad \delta = 2 + \frac{1}{3}\varepsilon, \tag{166}$$

from Eqs. (163), (164), (146), and (158), are all real. In addition, the first two exponents agree with the results given by Eqs. (126) and (128), provided the fixed-point value in Eq. (165) is substituted. For $\varepsilon = 0$ or $d = 6$, corresponding to $u_R^* = 0$, all the exponents recover their Gaussian fixed-point values listed in Table 1. This fact again shows that the fixed points, although imaginary, correctly describe the large-scale fluctuations at the instability point at which the real mean-field transition occurs. Moreover, using a finite-time scaling with the Monte Carlo RG method, we have found that an imaginary fixed point can affect the RG flow in a temperature-driven FOPT of the Potts model with $d = 2$ [80]. From these exponents, others can also be obtained. We return to the instability exponents in Section 8.

7.7 Finite-time scaling

Although the scaling and universality behavior found in the last section is similar to that for the critical phenomena, it may not be easily observable, because of the instability and the dynamic nature of the transition. An accessible method is to employ finite-time scaling, the efficacy of which has been proven for the critical phenomena [64, 65]. In this method, one varies the external field linearly through the transition point in order to probe the scaling behavior. In this section, we derive the finite-time scaling form for the FOPTs.

Let the rate R of the linear driving be renormalized as

$$R = Z_r R_R. \tag{167}$$

We find

$$Z_r = Z_\lambda^{-1} Z_\varphi^{-1/2} = Z_\varphi^{-1} Z_{\tilde\varphi}^{1/2}, \tag{168}$$

by assuming that both the bare and renormalized forms of the driving form, Eq. (48) with the λ included, are identical, such that

$$h_R = \lambda_R R_R t = Z_\varphi^{1/2} h = Z_\varphi^{1/2}\lambda R t, \tag{169}$$

using Eq. (136) and Eqs. (105) and (108). Although such driving breaks the time translational symmetry, it has been shown that this approach introduces a possible initial slip near criticality only, arising from nonequilibrium initial conditions that induce a new singularity [81]. In finite-time scaling, we always begin the driving far from the critical/instability point, as mentioned in Section 4.3. Consequently, the initial slip should have no effect, unless we intentionally begin the driving near the instability point to study it. If the initial slip is neglected, the driving does not induce any new singularity [66]. Accordingly, the three Z factors introduced in Section 7.3 suffice for curing all the intrinsic singularities. This is why Z_r is related to the previous factors, as indicated by Eq. (168). As λ_R and R_R are related, we choose R_R as a variable and express the RG equation for h_R as

$$\left(\mu\frac{\partial}{\partial\mu} + \gamma_r R_R\frac{\partial}{\partial R_R} + \beta\frac{\partial}{\partial u_R} - \frac{1}{2}\gamma_\varphi m_R\frac{\partial}{\partial m_R} - \frac{1}{2}\gamma_\varphi\right)h_R = 0, \tag{170}$$

with

$$\gamma_r = \mu\frac{\partial \ln R_R}{\partial\mu} = -\mu\frac{\partial \ln Z_r}{\partial\mu} = \gamma_\varphi - \frac{1}{2}\gamma_{\tilde\varphi}, \tag{171}$$

from Eqs. (167), (168), and (130). The solution at the fixed point is then

$$h_R(R_R, m_R, u_R^*) = \kappa^{\beta\delta/\nu} h_R(R_R\kappa^{-r_H}, m_R\kappa^{-\beta/\nu}, u_R^*), \tag{172}$$

with

$$r_H = \frac{d+6}{2} - \gamma_r^* = z + \frac{1}{2}(d + 2 - \eta) = z + \beta\delta/\nu, \tag{173}$$

which is obtained by noting that

$$\kappa\frac{dR_R(\kappa)}{d\kappa} = \gamma_r R_R(\kappa), \quad R_R(1) = R_R, \tag{174}$$

and $[R] = [h] - [\lambda t] = (d+6)/2$, using Table 2. We have also used Eqs. (146) and (156), and the solution of Eq. (174) at the fixed point. Equation (173) is simply Eq. (49), and Eq. (172) is simply another form of Eq. (50). In fact, we can derive an RG equation for m_R directly, with h_R as its variable [42]. Hence, we find

$$n_H = \beta\delta/(\nu r_H) = \frac{d+2-\eta}{d+2-\eta+2z},$$
$$n_m = \beta/(\nu r_H) = \frac{d-2+\eta}{d+2-\eta+2z}, \tag{175}$$

the one-loop ε expansions of which are

$$n_H = \frac{2}{3} - \frac{1}{54}\varepsilon, \quad n_m = \frac{1}{3} - \frac{7}{108}\varepsilon, \tag{176}$$

respectively, using Eq. (166), thereby recovering their mean-field values for $\varepsilon = 0$. Note that these hysteresis exponents have been found to be comparable with direct numerical solutions of Eqs. (1) and (9) [42]. This result again supports the relevance of the φ^3 theory to the FOPTs. We shall return to this comparison in Section 8.

7.8 Leading corrections to scaling

When the initial u_R lies near to u_R^* rather than at it, leading corrections to the exact scaling behavior exist [82], as shown in Eqs. (144) and (155).

Consider the external field for an instance and assume that β is given by Eq. (160). Let

$$\ln Z_\varphi(u_R) = -\int_{u_R^*}^{u_R} \frac{\mathrm{d}x}{\beta(x)}[\gamma_\varphi(x) - \eta], \tag{177}$$

$$m_R(u_R) = m_R Z_\varphi^{-1/2}(u_R), \tag{178}$$

$$\lambda_R(u_R) = \lambda_R \exp\left\{-\int_{u_R^*}^{u_R} \frac{\mathrm{d}x}{\beta(x)}[\gamma_\lambda(x) - z + 2]\right\}, \tag{179}$$

$$\tilde{u} = (u_R - u_R^*)\exp\left\{\int_{u_R^*}^{u_R} \mathrm{d}x \left[\frac{\beta'}{\beta(x)} - \frac{1}{x - u_R^*}\right]\right\}, \tag{180}$$

which are finite renormalizations that eliminate trivial deviations from the fixed point theory and correspond simply to a change of normalization of the different scaling variables [53]. Then, we assume

$$h_R(t, \lambda_R, m_R, u_R, \mu) = Z_\varphi^{-1/2}(u_R) h_R(t, \lambda_R(u_R), m_R(u_R), u_R^*, \mu) U(t, \lambda_R(u_R), m_R(u_R), \tilde{u}, \mu), \tag{181}$$

with the boundary condition $U(t, \lambda_R(u_R), m_R(u_R), 0, \mu) = 1$. We substitute the above equation into Eq. (135), yielding

$$\left[\mu\frac{\partial}{\partial\mu} + (z-2)\lambda_R\frac{\partial}{\partial\lambda_R} + \beta'\tilde{u}\frac{\partial}{\partial\tilde{u}} - \frac{1}{2}\eta m_R\frac{\partial}{\partial m_R}\right] U(t, \lambda_R(u_R), m_R(u_R), \tilde{u}, \mu) = 0, \tag{182}$$

$$\left[\mu\frac{\partial}{\partial\mu} + (z-2)\lambda_R\frac{\partial}{\partial\lambda_R} - \frac{1}{2}\eta m_R\frac{\partial}{\partial m_R} - \frac{1}{2}\eta\right] h_R(t, \lambda_R(u_R), m_R(u_R), u_R^*, \mu) = 0. \tag{183}$$

These equations can be solved again via the method of characteristics after expanding U in powers of $\tilde{u}$, with the result

$$h_R(t, \lambda_R, m_R, u_R) = Z_\varphi^{-1/2}(u_R)\kappa^{\beta\delta/\nu} h_R(\lambda_R t\kappa^z, m_R\kappa^{-\beta/\nu}, u_R^*)\left[1 + \sum_{s=1}^{\infty}\tilde{u}^s\kappa^{s\beta'} f_4(\lambda_R t\kappa^z, m_R\kappa^{-\beta/\nu})\right], \tag{184}$$

where f_4 is a scaling function and use has been made of Eqs. (156) and (157). The finite-time scaling form of Eq. (184) is

$$h_R(R, \lambda_R, m_R, u_R) = Z_\varphi^{-1/2}(u_R) R^{\beta\delta/(\nu r_H)} h_R(1, m_R R^{-\beta/(\nu r_H)}, u_R^*)\left[1 + \sum_{s=1}^{\infty}\tilde{u}^s R^{s\beta'/r_H} f_5(m_R R^{-\beta/(\nu r_H)})\right], \tag{185}$$

with another scaling function f_5.

Note that the exponent of the corrections, β', depends on the fixed point only and is, thus, universal. To one-loop order,

$$\beta' = \varepsilon, \tag{186}$$

from Eqs. (162) and (165). It is real. However, the derivative of γ_φ with respect to its argument at u_R^*,

$$\gamma_\varphi' = \frac{1}{3}u_R^* = \pm\mathrm{i}\frac{1}{3}\sqrt{\frac{2}{3}\varepsilon}, \tag{187}$$

from Eqs. (163) and (165), is imaginary. Expanding β and γ_φ to first order in $u_R - u_R^*$, we find from Eq. (177)

that

$$\ln Z_\varphi(u_R) = -\frac{\gamma'_\varphi}{\beta'}(u_R - u_R^*) = \mp \mathrm{i}\sqrt{\frac{2}{27\varepsilon}}(u_R - u_R^*), \tag{188}$$

which may be complex, depending on u_R.

8 Existing φ^3 theories, Yang–Lee edge singularity, and resummed instability exponents

We studied the field-theoretical RG theory of the φ^3 theory of the FOPTs in detail in the last section. In fact, Hamiltonians that possess such a cubic interaction have been utilized to model many phase transitions. Examples include the isotropic-to-nematic phase transition in liquid crystals [83, 84]; systems described by the Potts model [62, 84–86] and, particularly, the percolation problem [62, 63, 84], which is the single-state Potts model [87]; the Edwards-Anderson model of spin glasses [88, 89]; a large number of nonequilibrium systems [90, 91], such as dynamic isotropic percolation and directed percolation [92]; the Reggeon field theory for high-energy scattering amplitudes [93, 94], which falls into the same universality class as the directed percolation [95]; the Yang–Lee edge singularity [43] and its related problems, such as isotropic branched polymers in a good solvent and undirected lattice animals, Anderson localization, and directed branched polymers and directed lattice animals, which are related to the edge singularity in the $d+2$ [96], $d+2$ [97], and $d+1$ dimensions [98], respectively; as well as quantum field theory models in particle physics [99]. As regards φ^3 models that are directly related to that studied here, they have been classified into two categories depending on whether or not "unphysical" limits, such as a particular state number limit or a purely imaginary coupling constant, must be implemented [100, 101]. Field theories having real Hamiltonians and no particular state number limit have an unstable ground state and instanton solutions, such that a perturbation expansion is not an adequate approach [102]. Moreover, the ϕ^4 interaction becomes relevant as the spatial dimensionality is reduced from six [102]. These statements are not valid for theories in the second category. Thus, the perturbation series has oscillatory terms and, hence, is Borel summable [103, 104]. Further, the quartic interaction has been found to be irrelevant [103, 105, 106]. The Yang–Lee edge singularity belongs to this class and, thus, the ε expansion in the RG analysis provides good results [100, 101]. In the following, we show that the dynamics of FOPTs near their instability points falls into the same universality class as the Yang–Lee edge singularity, and we apply its extant results to extend our findings for the FOPTs.

8.1 Yang–Lee edge singularity

According to Yang and Lee [107], in order to study the problem of phase transitions, it is necessary to study the distribution of the roots of the grand partition function in the complex fugacity plane. Under a class of general conditions, these roots lie on a circle in the plane for the Ising model and its equivalent lattice gas model [108]. For the Ising model, the fugacity is proportional to $\exp(-2H)$ (note that our definition of H has absorbed the thermal factor) and, thus, the Lee–Yang circle theorem places the zeros at imaginary magnetic fields. For $T < T_c$, there are zeros at $H = 0$ in the thermodynamic limit and the magnetization as a function of H exhibits a jump at $H = 0$; while for $T > T_c$, there is a gap of width $2\mathrm{i}H_0(T)$, within which no zeros exist. It has been found that the distribution of the zeros is singular at the gap edge [109]. This Yang–Lee edge singularity is described by [43]

$$m = M - M_0 \sim (H - \mathrm{i}H_0)^\sigma, \tag{189}$$

with

$$\sigma = \frac{1}{\delta} = \frac{d-2+\eta}{d+2-\eta}, \tag{190}$$

where M_0 is the magnetization at the imaginary field $\mathrm{i}H_0$.

Consider a continuous-spin Ising model in an imaginary external field above its critical temperature, viz., Eq. (1), with an imaginary H and $r > 0$ [43, 98]. As there is no spontaneous symmetry breaking for $r > 0$, but only the imaginary external field, the shift in Eq. (4) can only be to an imaginary M induced by H. From Eqs. (6) and (7), it is then apparent that τ is real, but both h and g_3 are imaginary. Therefore, the leading infrared behavior of the Yang–Lee edge singularity is governed by Eq. (8), with purely imaginary g_3 and h [43]. A redefinition of φ to $\mathrm{i}\varphi$ [96], which is a dummy variable that will be integrated out, then returns the Hamiltonian to exactly the form of Eq. (8). Therefore, this singularity for $T > T_c$ is indeed described by the same model as the FOPTs below T_c. As a result, for $d > d_c = 6$, the classical mean-field theory results in $\sigma = 1/2$, from Eq. (190) and Table 1. For $d < 6$, the $\varepsilon = 6 - d$ expansions of the RG functions for the Yang–Lee edge singularity have been computed up to three loops from those of the Potts model. Their resummed exponents agree impressively with those of the high-temperature series analysis [110], even down to the exact result of $\sigma = -1/2$ for the one-dimensional Ising model, where $\varepsilon = 5$ [100, 101]. Further, the dynamic critical exponent for the Yang–Lee edge singularity has been computed up to two-loop order [111].

From the fixed point given by Eq. (165), it is apparent that the fixed-point value of u_R itself is, thus, imaginary. This again shows that the infrared behavior of the FOPT at its instability fixed point is simply described by the same field theory as that of the Yang–Lee edge singularity, albeit in opposite temperature ranges. We can then check that all our RG functions agree with previous results [62, 100, 101, 111]. Moreover, we can now employ these results to estimate the instability exponents, as shown in the following section.

8.2 Resummed instability exponents

The three- and two-loop results for η and z of the Yang–Lee edge singularity are [100, 101, 111]

$$\eta = -\frac{1}{9}\varepsilon - \frac{43}{3^6}\varepsilon^2 + \left(\frac{16\zeta(3)}{3^5} - \frac{8375}{2^2 3^{10}}\right)\varepsilon^3 + O(\varepsilon^4), \quad (191)$$

$$z = 2 - \frac{1}{18}\varepsilon + \left(\frac{241}{11664} - \frac{1}{8}\ln\frac{4}{3}\right)\varepsilon^2 + O(\varepsilon^3), \quad (192)$$

respectively, where ζ is the Riemann function. The former series has been resummed using a [2/1] Padé approximant, a [2/1] Padé–Borel method, and a conformal mapping technique, providing rather good estimates, even for $d = 1$ or $\varepsilon = 5$ [100, 101]. The latter has also been resummed using a [2/1] Padé approximant, with the aid of the z result for $d = 0$, given by

$$z(d = 0) = 2 - \frac{1}{2}[2 + \eta(d = 0)], \quad (193)$$

in which $\eta(d = 0)$ is obtained through a similar approximation to two-loop order [111]. Such a [2/1] Padé approximant to η has been performed using the exact result of $\eta = -1$ for $d = 1$, for the Yang–Lee edge singularity to two-loop order [110].

As we now have a three-loop order of η, we can form a [3/2] Padé approximant to η using the same exact result for $d = 1$. The result is

$$\eta = -\frac{\varepsilon}{9}\frac{1 - 0.908\varepsilon - 2.223\varepsilon^2}{1 - 1.439\varepsilon - 1.066\varepsilon^2}. \quad (194)$$

In Table 3, we list the η values for various d's, together with the averages of those from various other resummation methods [100, 101]. It is apparent that the former values are slightly larger than the latter for large values of d. This behavior is expected, as the value for $d = 1$ has been fixed. Accordingly, as our final estimates, the results from Refs. [100, 101] are retained for $d \geq 3$ and are averaged with the present result for $d = 2$, yielding a closer value to the $\eta(d = 2) = -0.78(2)$ obtained from the high-temperature series expansion [110]. From these values, we can then compute δ, using Eq. (158). In addition, Table 3 also presents the values of ν according to

$$\nu = \frac{2}{d - 2 + \eta}, \quad (195)$$

from Eq. (157), as it has been shown that $\beta = 1$ for the scalar φ^3 model [100, 101, 112]. For the same reason, from

$$\gamma = \beta(\delta - 1), \quad (196)$$

we conclude that γ is simply given by $\delta - 1$. However, the values of ν, γ, and even δ have a quite strange appearance for lower dimensions. In fact, as we are studying the field-driven case, we consider the field instead of the temperature deviations from the instability point. The corresponding relations are then

$$\xi \sim h_R^{-\nu/(\beta\delta)}, \quad \chi \sim h_R^{-\gamma/(\beta\delta)}, \quad (197)$$

with

$$\nu/(\beta\delta) = \frac{2}{d + 2 - \eta}, \quad \gamma/(\beta\delta) = 1 - \sigma, \quad (198)$$

from Eqs. (156), (190), and (196). These two exponent ratios, which correspond simply to ν and γ, respectively, in the context of branched polymers [96] and directed animals [98], appear normal, as is apparent from Table 3.

Equation (194) gives a slightly different η and, hence, z in $d = 0$ compared to the $z = 1.614$ value from the two-loop result [111]. As a result, the [2/1] Padé approximant to Eq. (192) becomes

$$z = 2 - \frac{\varepsilon}{18}\frac{1 + 1.790\varepsilon}{1 + 1.515\varepsilon}, \quad (199)$$

with the results for various d values listed in Table 3. These values also differ only slightly from those obtained from the two-loop $\eta(d = 0)$ [111].

As mentioned above, the [3/2] Padé approximant to η yields the smallest estimates for $d = 5$–3 and the second smallest for $d = 2$, as can be seen from Table 3. We also note that the direct [2/1] Padé approximant to η [100, 101] invariably produces the largest estimates in Table 3. This suggests a need for formation of a [1/1] Padé approximant to z, such that

$$z = 2 - \frac{\varepsilon}{18}\frac{1}{1 - 0.0153\varepsilon}. \quad (200)$$

The results of this approximant are, indeed, all larger than those from Eq. (199), although the true values may not necessarily lie between them. Nevertheless, we take their averages as our final estimates for z for $d = 5$–2, so as to account for possible bias due to the two-point Padé approximant, as seen in the estimates of η.

With knowledge of η and z, we can then compute the hysteresis exponents from Eqs. (173) and (175). The results are given in Table 3, where we have also shown their spreads due to η and/or z, as for δ and ν. Note that we have computed all other exponents from η and z,

Table 3 Instability exponents.

d	6[1]	5	4	3	2	1	0
η[2]	0	-0.157	-0.351	-0.561	-0.778	-1[3]	-1.224
η[4]	0	-0.147 ± 0.002	$-0.329^{+0.012}_{-0.013}$	$-0.527^{+0.029}_{-0.033}$	$-0.736^{+0.053}_{-0.061}$	$-0.952^{+0.083}_{-0.098}$	
η[5]	0	-0.147 ± 0.002	$-0.329^{+0.012}_{-0.013}$	$-0.527^{+0.029}_{-0.033}$	$-0.747^{+0.064}_{-0.050}$	-1[3]	-1.224
δ[6]	2	2.505 ± 0.003	$3.788^{-0.034}_{+0.038}$	$11.685^{-0.733}_{+0.951}$	$-6.355^{-0.502}_{+0.336}$	-2	-1[7]
ν[6]	1/2	0.701 ± 0.0005	$1.197^{-0.009}_{+0.009}$	$4.228^{-0.244}_{+0.317}$	$-2.677^{-0.251}_{+0.168}$	-1	-0.620
$\nu/(\beta\delta)$[6]	1/4	0.280 ± 0.0001	0.316 ± 0.0006	0.362 ± 0.002	$0.421^{+0.006}_{-0.004}$	0.5	0.620
$\gamma/(\beta\delta)$[6]	1/2	0.580 ± 0.0001	0.684 ± 0.0006	0.819 ± 0.001	1	1.25	1.620
z[8]	2	1.938	1.874	1.809	1.743	1.677	1.612
z[9]	2	1.944	1.885	1.825	1.763	1.699	1.633
z[5]	2	1.941 ± 0.003	1.880 ± 0.006	1.817 ± 0.008	1.753 ± 0.010	1.677	1.612
r_H[6]	6	5.512 ± 0.003	$5.038^{-0.006}_{+0.007}$	$4.572^{-0.015}_{+0.017}$	$4.117^{-0.032}_{+0.025}$	3.678	3.224
n_H[6]	2/3	0.648 ± 0.0004	0.627 ± 0.001	0.603 ± 0.003	$0.575^{+0.004}_{-0.005}$	0.544	0.5
n_m[6]	1/3	$0.259^{+0.0002}_{-0.0003}$	$0.166^{+0.001}_{-0.002}$	$0.0516^{+0.0033}_{-0.0039}$	$-0.0905^{+0.0073}_{-0.0057}$	-0.272	-0.5
n_H[10]	0.654(8)	0.645(3)	0.625(12)	0.595(30)			
n_m[10]	0.34(6)	0.27(4)	0.17(8)				

[1] Mean-field results.
[2] Equation (194) using the [3/2] Padé approximant.
[3] Exact result [43].
[4] Reference [100, 101] (quoted errors reflect the spread in different resummations).
[5] Final estimates (quoted errors reflect the spread in different resummations).
[6] Quoted errors reflect the corresponding spreads in η and/or z in the final estimates.
[7] Exact result [96, 111].
[8] Equation (199) using the [2/1] Padé approximant.
[9] Equation (200) using the [1/1] Padé approximant.
[10] Numerical results [42].

rather than resumming their respective ε series, as only these two exponents are independent for the φ^3 theory.

Table 3 also includes the numerical results of direct numerical solutions of Eqs. (1) and (9) [42]. The agreement between the theoretical and numerical results is remarkable. In fact, as noted above, even the one-loop results agree well with these results [42], although high-order results without resummations do not exhibit such agreements, similar to the critical phenomenon case. Of course, higher-order theoretical and further numerical results are desirable. Nevertheless, this agreement again confirms the relevance of the φ^3 theory to the FOPTs. Note that, although we only compare the hysteresis exponents in Table 3, the static exponents and the dynamic exponent z can also be estimated [80]. As these exponents comprise the hysteresis exponents and are derived directly from the RG theory, they are more fundamental. Note, however, that they are irrelevant to the transition at the conventional equilibrium transition point.

9 Discussion

We have studied the φ^3 theory for the FOPTs in detail. The compelling evidence for scaling in driven FOPTs mentioned in Section 1 and demonstrated in this paper strongly supports the relevance of the theory and its infrared stable fixed points to the scaling. We have also shown in Section 7.6 and, in particular, through Eq. (161), that the fixed points are indeed reached independently of the initial coupling when $\kappa \to 0$. However, as the fixed points are imaginary, one may wonder how such imaginary fixed points can be reached from the real physical world or, more specifically, how they can be reached for an RG flow starting from real physical conditions. This question casts doubt on the extent of the relevancy. Another possible interpretation is that the scaling behavior is merely a crossover affected by the φ^3. For the fixed points to affect the flows, however, the latter should flow sufficiently close to the former. Yet, as the fixed points are far from the real physical parameters for practical ε's at least, it is hardly possible for them to leave their trace in real measurements. On the other hand, in simulations at least [42], scaling is easily found in all spatial dimensions, with no detectable indication of difficulty for lower dimensions, in which the fixed points are farther away. Moreover, as has been noted above, the determined hysteresis exponents agree well with those of the φ^3 theory. Therefore, such a crossover is unlikely, if not rule out, to occur. We also note that crossover of the

pseudo-critical phenomena [61] cannot be a candidate either, as the theory is irrelevant even at the mean-field level, as shown in Section 4.3. This is despite the fact that the hysteresis exponents that would be predicted by the theory, $n_H = 3/5$ for $d \geq 4$ from Table 1 and $n_H = 0.5493(12)$ in $d = 3$ [66], are not far from those listed in Table 3.

In order to observe the manner in which the fixed points are reached explicitly, we now study the flow equations in detail, by regarding them as rigorous equations. Consider the flow of the coupling constant, Eq. (137c), with $\beta(u_R)$ given by Eq. (162). This equation is solved analytically by

$$u_R^2(\kappa) = \frac{2\varepsilon u_R^2}{3u_R^2\,(\kappa^\varepsilon - 1) + 2\varepsilon\kappa^\varepsilon}, \tag{201}$$

for initial $u_R = u_R(\kappa = 1)$. It is apparent that $u_R^2(\kappa)$ converges to u_R^{*2} and 0 correctly for $\kappa \to 0$, when ε is positive and negative, corresponding to $d < 6$ and $d > 6$, respectively. The denominator of the solution is equal to zero at a specific κ_0, satisfying

$$\kappa_0^\varepsilon = \frac{3u_R^2}{3u_R^2 + 2\varepsilon} \quad \text{or} \quad \kappa_0 = \mathrm{e}^{-\mathrm{sgn}(\varepsilon)2/(3u_R^2)} \tag{202}$$

to $O(1)$, where sgn is the sign function. Because the running variable κ and the dimension ε are real, only a real u_R yields a real κ_0. Note that, for $\varepsilon < 0$, $\kappa_0 > 1$. As a result, κ_0 does not affect the flow from $\kappa = 1$ to $\kappa = 0$ and, hence, any initial u_R converges continuously to the Gaussian fixed point, as expected and as shown in Fig. 3(a). However, for $\varepsilon > 0$, $\kappa_0 < 1$, and the flow diverges at κ_0 for a real u_R. Therefore, κ_0 is the branch point of $u_R(\kappa)$. Yet, after approaching infinity, $u_R(\kappa)$ acquires an infinite imaginary part that then converges to the fixed-point values, as shown in Figs. 3(b) and (c). It appears that the divergence spontaneously triggers an imaginary part in $u_R(\kappa)$, such that the purely imaginary fixed point can still be reached, as indicated by the solution given in Eq. (201). Conversely, in order to acquire an imaginary part to reach the imaginary fixed point, one may imagine that the initial real flow must enter a divergent "no-man's land." However, the flow trajectory jumps abruptly from the real to the imaginary plane, as illustrated in Fig. 3(a). The flow trajectory does becomes continuous once u_R possesses an imaginary part, however, regardless of its smallness. The only difference for different values of the imaginary part is the magnitude of the convolutions shown in Fig. 3(a). The smaller the former, the larger the latter. Further, no qualitative difference appears between different spatial dimensions below $d_c = 6$; the difference is only the value of κ_0 and, again, the magnitude of the convolution. We have checked that the divergence remains when the contribution from the

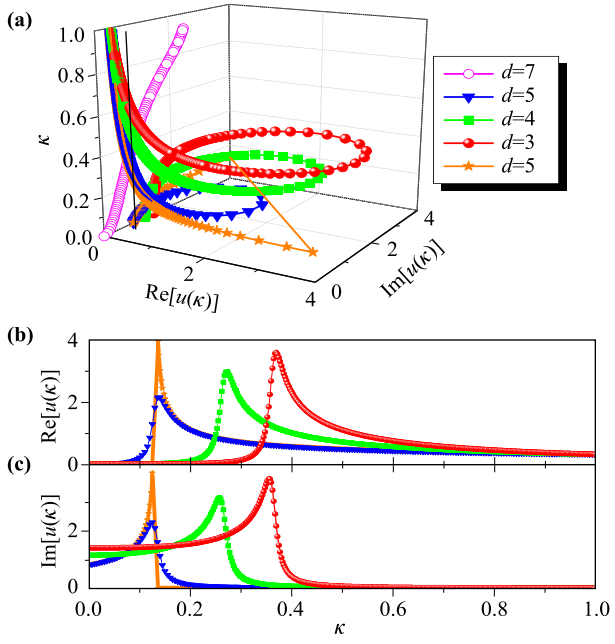

Fig. 3 **(a)** RG flows from $\kappa = 1$ to $\kappa = 0$ of the coupling for a real [$d = 5$ (*stars*)] and a complex (all the others with $d < 6$) initial coupling, $u_R^2 = 0.1$ and $u_R^2 = 0.1 + 0.01\mathrm{i}$, respectively. The flow for $d = 7$ has $u_R^2 = 0.1 + 2\mathrm{i}$. For clarity of illustration, we have cut off the large values of the flow with a real initial value at $d = 5$ (*stars*). **(b)** and **(c)** show the projections of the flows in (a) to the real and imaginary plane, respectively, in the absence of the flow for $d = 7$. The legend applies to all panels.

two-loop order is considered; however, in that case one must resort to numerical solutions. As other variables depend on $u_R(\kappa)$, they also exhibit a similar feature.

Therefore, it is apparent that the fixed points can be continuously reached irrespective of the magnitude of the initial coupling constant, if the latter possesses an imaginary value. In contrast, for purely real initial values to converge to the imaginary fixed points, the RG flows must diverge at a finite scale in order to acquire an imaginary part. At present, we can speculate on the reason for the imaginary nature of the fixed points. As noted in Ref. [42], it has been shown that the free energy of the metastable states is complex [44, 49, 50]. In fact, as the φ^3 theory is not bounded from below, an analytical continuation must be performed when computing the free energy [Eq. (2)]. In particular, as the free energy diverges for negative φ, the integration in this region must be deformed to the imaginary axis. Therefore, one should set $\varphi \to \mathrm{i}\varphi$ in the integrand, which naturally yields $\mathrm{i}g_3$. Consequently, an imaginary fixed point appears to be a natural and plausible choice for controlling the local unstable transition near the instability point of an FOPT, possibly countering the intuition that only real values constitute physics. It can also be imagined that the divergence at a

finite scale of a real initial coupling should also be pertinent to this behavior. Moreover, note that the negative φ is simply the direction of the FOPT rather than the third-order transition. However, until a solid solution to the divergence and imaginary problems is obtained, the present theory will remain a hypothesis, although we have clearly shown its relevance to the FOPTs.

10 Summary

We have basically repeated the entire theory of critical phenomena in the context of φ^3 theory for FOPTs, in an attempt to stress both their similarities and differences. Instead of lengthy proofs, we have attempted to illustrate known general rules with direct examples. We have studied the mean-field theory, the Gaussian theory, the perturbation expansion, and the RG theory in detail. Finite-time scaling and leading corrections to scaling have also been considered. We have also touched on the Yang–Lee edge singularity and employed its results to improve our estimates of the instability exponents. The main results are as follows.

In the mean-field approximation, we have shown that, for a scalar ϕ^4 model below its T_c, the FOPT at the spinodal point driven by an external field is governed by the transition at the instability point of the corresponding φ^3 model. This is despite the fact that the FOPT and the third-order transition between the two states described by the φ^3 theory fall into opposite ground states and appear different. Via finite-time scaling, both numerical results and analytical solutions indeed confirm the relevance of the instability exponents rather than the critical exponents. The Gaussian theory clearly shows that both the correlation length and the correlation time diverge at the instability point, similar to the critical phenomenon case. In addition, all the mean-field instability exponents have been derived conventionally. The perturbation expansion around the mean-field theory demonstrates that infrared divergences plague and, thus, necessitate an RG theory for $d \leq 6$, as expected. Further, the mean-field results survive for $d > 6$ and outside the unstable region only for $d < 6$. Power counting analysis shows that, in the unstable region and for $d < 6$, the effective local field φ^3 theory does reproduce the sum of the most divergent contributions order by order in the mean-field expansion. Detailed computations of the renormalization functions to one-loop order and derivations and solutions of the RG equations for a general vertex function and the magnetic field show unambiguously that a pair of complex-conjugate imaginary fixed points exist. These points are infrared stable, similar to the critical fixed point; thus, controlling the large-scale universal behavior. Exact scaling forms and scaling laws among the instability exponents have been derived and the latter have been computed to one-loop order. In six dimensions, these instability exponents recover the mean-field exponents, which again shows that the fixed points, albeit imaginary, correctly describe the large-scale fluctuations at the instability point at which the real mean-field transition occurs. We have computed two particular explicit forms of the renormalized massless two-point response function to one-loop order. The finite-time scaling form and associated exponents have also been derived, which serve as an accessible method of probing the instability point. We have derived the leading corrections to the scaling and confirmed that they are controlled by a universal exponent. We have also shown that the infrared behavior of the φ^3 theory of the FOPTs falls within the same universality class as the Yang–Lee edge singularity, although the former is for $T < T_c$ while the latter is for $T > T_c$. This implies that the ε expansions can be trusted and the ϕ^4 interaction is irrelevant. Moreover, the two- and three-loop-order exponents of the edge singularity have been employed to estimate the instability exponents. The outcomes agree well with previous numerical results, again confirming the relevance of the φ^3 theory to FOPTs. It appears that this relevancy is unlikely to be simply due to a crossover behavior. On the one hand, although the RG flow with a purely real initial coupling diverges at a finite scale, an imaginary part is generated beyond that scale and the imaginary fixed point can then be reached. On the other hand, if the initial coupling acquires a finite imaginary part of any magnitude, true asymptotic behavior can surely be established. We speculate that the imaginary nature of the fixed points may be a natural consequence of the instability of the φ^3 theory. However, further studies are clearly required.

We conclude, therefore, that the instability fixed points of the φ^3 theory, together with their instability exponents, are clearly relevant to the scaling and universality behavior exhibited by FOPTs near their instability points. Further studies are desirable in order to dispel possible concern regarding the instability point, to clarify the divergence of the RG flow and the imaginary nature of the fixed points, to search for new classes, and to find experimental evidence to support these claims.

Appendix A Supersymmetry action

Following Ref. [53], another method of managing the Jacobian, Eq. (15), is to use the Gaussian integral of the anticommuting classical Grassmann variables

$$\det E = \int \mathcal{D}c\mathcal{D}\tilde{c} \exp\left(\tilde{c}Ec\right) \tag{A1}$$

to express the generating functional as

$$Z[J,\tilde{J}]=\int \mathcal{D}\phi\mathcal{D}\tilde{\phi}\mathcal{D}c\mathcal{D}\tilde{c}\exp\left[-\mathcal{L}+\int \mathrm{d}x\left(J\phi+\tilde{J}\tilde{\phi}\right)\right], \tag{A2}$$

with the effective action

$$\mathcal{L}[\phi,\tilde{\phi},c,\tilde{c}]=\int \mathrm{d}x\left[\tilde{\phi}\left(\frac{\partial\phi}{\partial t}+\lambda\frac{\delta\mathcal{H}}{\delta\phi}\right)-\lambda\tilde{\phi}^2 -\tilde{c}\left(\frac{\partial}{\partial t}+\lambda\frac{\delta^2\mathcal{H}}{\delta\phi^2}\right)c\right], \tag{A3}$$

where

$$c_nc_{n'}+c_{n'}c_n=0,\quad \text{for any } n,n', \tag{A4}$$

with c_n representing c or $\tilde{c}$. Note that the local nature of $\mathcal{H}$ has been used.

Introducing two new Grassmann variables θ and $\tilde{\theta}$ as additional coordinates to x and defining a superfield ψ by

$$\psi(x,\theta,\tilde{\theta})=\phi(x)+\sqrt{\lambda}\tilde{\theta}c(x)+\sqrt{\lambda}\tilde{c}(x)\theta+\lambda\tilde{\theta}\theta\tilde{\phi}(x), \tag{A5}$$

the action (A3) can be expressed in the following remarkably simple form:

$$\mathcal{L}[\psi]=\int \mathrm{d}\theta\mathrm{d}\tilde{\theta}\mathrm{d}t\left\{\frac{1}{\lambda}\int \mathrm{d}\boldsymbol{x}\tilde{D}\psi D\psi+\mathcal{H}[\psi]\right\}, \tag{A6}$$

with the definitions

$$\tilde{D}\equiv\frac{\partial}{\partial\theta},\quad D\equiv\frac{\partial}{\partial\tilde{\theta}}-\theta\frac{\partial}{\partial t}, \tag{A7}$$

by noting that the integrations over θ and $\tilde{\theta}$ select the term proportional to $\theta\tilde{\theta}$ because of their anticommuting character, similar to Eq. (A4). For example,

$$\int \mathrm{d}\theta\mathrm{d}\tilde{\theta}\mathrm{d}t\mathcal{H}[\psi]=\lambda\int \mathrm{d}x\left\{\frac{\delta\mathcal{H}[\phi]}{\delta\phi(x)}-\tilde{c}(x)\frac{\delta^2\mathcal{H}[\phi]}{\delta\phi(x)^2}c(x)\right\}.$$

The action (A6) is invariant under a supersymmetry transformation

$$\delta\psi=\epsilon\left(\frac{\partial}{\partial\theta}+\tilde{\theta}\frac{\partial}{\partial t}\right)\psi \tag{A8}$$

or, in component form,

$$\begin{aligned}&\delta\phi=\sqrt{\lambda}\tilde{c}\epsilon,\quad \delta\tilde{c}=0,\\ &\delta c=\left(\tilde{\phi}-\frac{1}{\sqrt{\lambda}}\frac{\partial\phi}{\partial t}\right)\epsilon,\quad \delta\tilde{\phi}=\frac{1}{\sqrt{\lambda}}\frac{\partial\tilde{c}}{\partial t}\epsilon,\end{aligned} \tag{A9}$$

which mix commuting and anticommuting fields, where ϵ is an infinitesimal anticommuting number here. This supersymmetry yields Ward–Takahashi identities that result in the fluctuation-dissipation theorem, Eq. (34), when combined with causality [53]. The supersymmetry also ensures that the equal-time correlation functions converge to the corresponding static functions at large time values [53].

Renormalization can be directly performed to the action (A6) [53]. Direct power counting confirms that the static and supersymmetry dynamic theories have the same upper critical dimension. The supersymmetry then yields the renormalized action of the form

$$\mathcal{L}_R[\psi_R]=\int \mathrm{d}\theta\mathrm{d}\tilde{\theta}\mathrm{d}t\left\{\frac{1}{\lambda_R}Z_\lambda\int \mathrm{d}\boldsymbol{x}\tilde{D}\psi_R D\psi_R+\mathcal{H}_R[\psi_R]\right\}. \tag{A10}$$

Therefore, only one new renormalization factor besides the static factors must be introduced. Equation (A10) also implies that the form of the Langevin equation, Eq. (9), is retained after renormalization.

Appendix B Useful formulas and relevant results

A useful dimensionally regulated integral is [79]

$$\int\frac{\mathrm{d}\overline{\boldsymbol{k}}}{(\tau+2\boldsymbol{p}\cdot\boldsymbol{k}+\boldsymbol{k}^2)^n}=N_d\frac{\Gamma\left(\frac{d}{2}\right)\Gamma\left(n-\frac{d}{2}\right)}{2\Gamma(n)}(\tau-\boldsymbol{p}^2)^{\frac{d}{2}-n}, \tag{B1}$$

where

$$N_d=\frac{2}{(4\pi)^{\frac{d}{2}}\Gamma\left(\frac{d}{2}\right)} \tag{B2}$$

is the surface area of a d-dimensional sphere divided by $(2\pi)^d$ and the Euler Gamma function $\Gamma(z)$ satisfies

$$\Gamma(z+1)=z\Gamma(z) \tag{B3}$$

and has poles at zero and negative integers. This can be seen from its expansion [113]

$$\Gamma(-n+\varepsilon)=\frac{(-1)^n}{n!}\left[\frac{1}{\varepsilon}+\psi_1(n+1)+O(\varepsilon)\right] \tag{B4}$$

for zero (note that $0!=1$) and integer n for small ε, where

$$\psi_1(z)=\frac{1}{\Gamma(z)}\frac{\mathrm{d}\Gamma(z)}{dz}=-\gamma-\frac{1}{z}+\sum_{\iota=1}^{n}\left(\frac{1}{\iota}-\frac{1}{z+\iota}\right), \tag{B5}$$

which, for the integer n, becomes

$$\psi_1(n+1)=-\gamma+\sum_{\iota=1}^{n}\frac{1}{\iota}, \tag{B6}$$

with the Euler constant $\gamma = -\psi_1(1) = 0.577$. Using Eqs. (B3) and (B4) at $n = 0$, one obtains the expansion

$$\Gamma(1+\varepsilon) = \varepsilon\Gamma(\varepsilon) = 1 - \gamma\varepsilon + O(\varepsilon^2). \tag{B7}$$

From Eq. (B5), one also obtains

$$\begin{aligned}\Gamma\left(\frac{1}{2}+\varepsilon\right) &= \Gamma\left(\frac{1}{2}\right) + \Gamma\left(\frac{1}{2}\right)\psi_1\left(\frac{1}{2}\right)\varepsilon + O(\varepsilon^2),\\ &= \sqrt{\pi}\left[1 - (\gamma + 2\ln 2)\varepsilon\right] + O(\varepsilon^2),\end{aligned} \tag{B8}$$

where $\Gamma(1/2) = \sqrt{\pi}$ and $\psi_1(1/2) = -\gamma - 2\ln 2$.

A useful formula to calculate graphs is to use the Feynman parameters x_ι to write

$$\frac{1}{\prod_\iota^n A_i^{n_\iota}} = \frac{\Gamma(\alpha)}{\prod_\iota^n \Gamma(\alpha_\iota)} \int_0^1 \prod_{\iota=1}^n \left(\mathrm{d}x_\iota x_\iota^{n_\iota - 1}\right) \frac{\delta(1-x)}{\left(\sum_\iota^n x_\iota A_\iota\right)^\alpha}, \tag{B9}$$

where $\alpha = \sum \alpha_\iota$ and $x = \sum x_\iota$. Using Eqs. (B9), (B1), and the integral

$$\int_0^1 x^{\mu-1}(1-x)^{\nu-1}\mathrm{d}x = \frac{\Gamma(\mu)\Gamma(\nu)}{\Gamma(\mu+\nu)}, \tag{B10}$$

one finds

$$\int \mathrm{d}\bar{\boldsymbol{k}} \frac{1}{\boldsymbol{k}^{2n_1}(\tau + \boldsymbol{k}^2)^n} = \frac{1}{2} N_d \tau^{\frac{d}{2}-n-n_1} \frac{\Gamma\left(\frac{d}{2} - n_1\right)\Gamma\left(n + n_1 - \frac{d}{2}\right)}{\Gamma(n)}, \tag{B11}$$

$$\int \mathrm{d}\bar{\boldsymbol{k}} \frac{1}{\boldsymbol{k}^{2n_1}(\boldsymbol{p} - \boldsymbol{k})^{2n_2}} = \frac{1}{2} N_d \left(\boldsymbol{p}^2\right)^{d/2-n_1-n_2} \frac{\Gamma\left(\frac{d}{2}\right)\Gamma\left(\frac{d}{2} - n_1\right)\Gamma\left(\frac{d}{2} - n_2\right)\Gamma\left(n_1 + n_2 - \frac{d}{2}\right)}{\Gamma(n_1)\Gamma(n_2)\Gamma(d - n_1 - n_2)}. \tag{B12}$$

Again, using Eqs. (B9) and (B1), one obtains

$$I_1(\boldsymbol{p}) = \int \mathrm{d}\bar{\boldsymbol{k}} \frac{1}{\boldsymbol{k}^2\left[\boldsymbol{k}^2 + (\boldsymbol{p} - \boldsymbol{k})^2\right]^2} = \frac{1}{2} N_d A \left(\boldsymbol{p}^2\right)^{d/2-3} \Gamma\left(\frac{d}{2}\right)\Gamma\left(3 - \frac{d}{2}\right), \tag{B13}$$

$$I_2(\boldsymbol{p}) = \int \mathrm{d}\bar{\boldsymbol{k}} \frac{1}{\boldsymbol{k}^2(\boldsymbol{p} - \boldsymbol{k})^2\left[\boldsymbol{k}^2 + (\boldsymbol{p} - \boldsymbol{k})^2\right]} = \frac{1}{2} N_d B \left(\boldsymbol{p}^2\right)^{d/2-3} \Gamma\left(\frac{d}{2}\right)\Gamma\left(3 - \frac{d}{2}\right), \tag{B14}$$

$$I_3(\boldsymbol{p}_1, \boldsymbol{p}_2) = \int \mathrm{d}\bar{\boldsymbol{k}} \frac{1}{\boldsymbol{k}^2(\boldsymbol{p}_1 - \boldsymbol{k})^2(\boldsymbol{p}_2 + \boldsymbol{k})^2} = \frac{1}{2} N_d C \mu^{d-6} \Gamma\left(\frac{d}{2}\right)\Gamma\left(3 - \frac{d}{2}\right), \tag{B15}$$

where $\boldsymbol{p}_1 = \mu\boldsymbol{k}_1$, $\boldsymbol{p}_2 = \mu\boldsymbol{k}_2$, and

$$A = \int_0^1 \mathrm{d}x \frac{x^{\frac{d}{2}-2}}{(1+x)^{d-3}}, \tag{B16}$$

$$B = \int_0^1 \mathrm{d}x \int_0^{1-x} \mathrm{d}y \frac{(x+y)^{\frac{d}{2}-3}(1-y)^{\frac{d}{2}-3}}{(1+x)^{d-3}}, \tag{B17}$$

$$C = \int_0^1 \mathrm{d}x \int_0^{1-x} \mathrm{d}y \left[x\boldsymbol{k}_1 + y\boldsymbol{k}_2^2 - (x\boldsymbol{k}_1 - y\boldsymbol{k}_2)^2\right]^{\frac{d}{2}-3}. \tag{B18}$$

For small $\varepsilon = 6 - d$, one finds from Eqs. (B3), (B4), and (B7) that

$$\Gamma\left(\frac{d}{2}\right)\Gamma\left(3 - \frac{d}{2}\right) = \frac{4}{\varepsilon}\left[1 - \frac{3}{4}\varepsilon + O(\varepsilon^2)\right], \tag{B19}$$

which has an ε pole. Owing to this pole, one can simply set $d = 6$ in the integrands of A, B, and C, as only first-order poles appear in the ε expansion to one-loop order. As a result,

$$A = \frac{1}{8} + O(\varepsilon), \quad B = \frac{1}{4} + O(\varepsilon), \quad C = \frac{1}{2} + O(\varepsilon). \tag{B20}$$

Therefore,

$$I_1(\boldsymbol{p}) = \frac{1}{4\varepsilon}\left[1 + O(\varepsilon)\right] N_d \left(\boldsymbol{p}^2\right)^{d/2-3}, \tag{B21}$$

$$I_2(\boldsymbol{p}) = \frac{1}{2\varepsilon}\left[1 + O(\varepsilon)\right] N_d \left(\boldsymbol{p}^2\right)^{d/2-3}, \tag{B22}$$

$$I_3(\boldsymbol{p}_1, \boldsymbol{p}_2) = \frac{1}{\varepsilon}\left[1 + O(\varepsilon)\right] N_d \mu^{d-6}. \tag{B23}$$

Note added in proof. The problem of the divergence and imaginariness of the fixed point was studied in Ref. [114].

Acknowledgements This work was supported by the National Natural Science Foundation of China (Grant No. 10625420).

References and notes

1. P. Ehrenfest, Phasenumwandlungen im üblichen und erweiterten Sinn, classifiziert nach dem entsprechenden Singularitäten des thermodynamischen Potentiales, Comm. Kamerlingh Onnes Lab., University of Leiden, Suppl. 75b (1933) [*Proc. Acad. Sci. Amsterdam* 36, 153 (1933)]

2. M. E. Fisher, The theory of equilibrium critical phenomena, *Rep. Prog. Phys.* 30(2), 615 (1967)
3. T. Andrews, The Bakerian lecture: On the continuity of the gaseous and liquid states of matter, *Philos. Trans. R. Soc. Lond.* 159(0), 575 (1869)
4. K. G. Wilson, Renormalization group and critical phenomena (I), *Phys. Rev. B* 4(9), 3174 (1971)
5. K. G. Wilson, Renormalization group and critical phenomena (II): Phase-space cell analysis of critical behavior, *Phys. Rev. B* 4(9), 3184 (1971)
6. K. G. Wilson and J. Kogut, The renormalization group and the e expansion, *Phys. Rep. C* 12(2), 75 (1974)
7. M. E. Fisher, The renormalization group in the theory of critical behavior, *Rev. Mod. Phys.* 46(4), 597 (1974)
8. H. E. Stanley, Scaling, universality, and renormalization: Three pillars of modern critical phenomena, *Rev. Mod. Phys.* 71(2), S358 (1999)
9. For a recent review, see, M. Barmatz, I. Hahn, J. A. Lipa, and R. V. Duncan, Critical phenomena in microgravity: Past, present, and future, *Rev. Mod. Phys.* 79(1), 1 (2007)
10. J. D. Gunton and D. Droz, Introduction to the Theory of Metastable and Unstable States, Berlin: Springer, 1983
11. J. D. Gunton, M. San Miguel, and P. S. Sahni, in: Phase Transitions and Critical Phenomena, eds. C. Domb and J. L. Lebowitz, Vol. 8, London: Academic, 1983
12. K. Binder, Theory of first-order phase transitions, *Rep. Prog. Phys.* 50(7), 783 (1987)
13. P. G. Debenedetti, Metastable Liquids, Princeton: Princeton University, 1996
14. J. van der Waals, On the continuity of the gaseous and liquid state, Thesis, Leiden, 1873 (unpublished)
15. J. C. Maxwell, Scientific Papers, New York: Dover, 1965, p. 425
16. J. W. Gibbs, The Collective Works of J. Willard Gibbs, Vol. 1, New York: Longman, 1931
17. J. D. Gunton, Homogeneous nucleation, *J. Stat. Phys.* 95(5/6), 903 (1999)
18. D. W. Oxtoby, Nucleation of first-order phase transitions, *Acc. Chem. Res.* 31(2), 91 (1998)
19. R. B. Sear, Nucleation: Theory and applications to protein solutions and colloidal suspensions, *J. Phys.: Condens. Matter* 19, 033101 (2007)
20. K. Binder and P. Fratzl, in: Phase Transformations in Materials, ed. G. Kostorz, Weinheim: Wiley, 2001
21. J. S. Langer, M. Baron, and H. D. Miller, New computational method in the theory of spinodal decomposition, *Phys. Rev. A* 11(4), 1417 (1975)
22. K. Binder, "Clusters" in the Ising model, metastable states and essential singularity, *Ann. Phys.* 98(2), 390 (1976)
23. K. Binder and D. Stauffer, Statistical theory of nucleation, condensation and coagulation, *Adv. Phys.* 25(4), 343 (1976)
24. F. Zhong, Instability points and spinodal points, 2010 (unpublished)
25. B. Nienhuis and M. Nauenberg, First-order phase transitions in renormalization-group theory, *Phys. Rev. Lett.* 35(8), 477 (1975)
26. M. E. Fisher and A. N. Berker, Scaling for first-order phase transitions in thermodynamic and finite systems, *Phys. Rev. B* 26(5), 2507 (1982)
27. A. J. Bray, Theory of phase-ordering kinetics, *Adv. Phys.* 43, 357 (1994), reprinted as *Adv. Phys.* 51, 481 (2002), and references therein
28. J. Marro, J. L. Lebowitz, and M. H. Kalos, Computer simulation of the time evolution of a quenched model alloy in the nucleation region, *Phys. Rev. Lett.* 43(4), 282 (1979)
29. P. C. Hohenberg and B. I. Halperin, Theory of dynamic critical phenomena, *Rev. Mod. Phys.* 49(3), 435 (1977)
30. J. X. Zhang and X. J. Li, A new method for interface dynamic investigation in solid state phase transformations, *Acta Sci. Nat. Uni. Sun.* 2, 45 (1985)
31. M. Rao, H. R. Krishnamurthy, and R. Pandit, Hysteresis in model spin systems, *J. Phys.: Condens. Matter* 1(45), 9061 (1989)
32. M. Rao, H. R. Krishnamurthy, and R. Pandit, Magnetic hysteresis in two model spin systems, *Phys. Rev. B* 42(1), 856 (1990)
33. F. Zhong, J. X. Zhang, and G. G. Siu, Dynamic scaling of hysteresis in a linearly driven system, *J. Phys.: Condens. Matter* 6(38), 7785 (1994)
34. F. Zhong and J. X. Zhang, Scaling of thermal hysteresis with temperature scanning rate, *Phys. Rev. E* 51(4), 2898 (1995)
35. F. Zhong, J. X. Zhang, and X. Liu, Scaling of hysteresis in the Ising model and cell-dynamical systems in a linearly varying external field, *Phys. Rev. E* 52(2), 1399 (1995)
36. J. X. Zhang, P. C. W. Fung, and W. G. Zeng, Dissipation function of the first-order phase transformation in solids via internal-friction measurements, *Phys. Rev. B* 52(1), 268 (1995), and references therein
37. J. X. Zhang, Z. H. Yang, and P. C. W. Fung, Dissipation function of the first-order phase transformation in VO_2 ceramics by internal-friction measurements, *Phys. Rev. B* 52(1), 278 (1995)
38. J. X. Zhang, F. Zhong, and G. G. Siu, The scanning-rate dependence of energy dissipation in first-order phase transition of solids, *Solid State Commun.* 97(10), 847 (1996)
39. K. Chakrabarti and M. Acharyya, Dynamic transitions and hysteresis, *Rev. Mod. Phys.* 71(3), 847 (1999)

40. F. Zhong and J. X. Zhang, Renormalization group theory of hysteresis, *Phys. Rev. Lett.* 75(10), 2027 (1995)
41. F. Zhong, Monte Carlo renormalization group study of the dynamic scaling of hysteresis in the two-dimensional Ising model, *Phys. Rev. B* 66, 060401(R) (2002)
42. F. Zhong and Q. Z. Chen, Theory of the dynamics of first-order phase transitions: Unstable fixed points, exponents, and dynamical scaling, *Phys. Rev. Lett.* 95(17), 175701 (2005)
43. M. E. Fisher, Yang–Lee edge singularity and ϕ^3 field theory, *Phys. Rev. Lett.* 40(25), 1610 (1978)
44. J. S. Langer, Theory of the condensation point, *Ann. Phys.* 41(1), 108 (1967)
45. O. Penrose and J. L. Lebowitz, Rigorous treatment of metastable states in the van der Waals–Maxwell theory, *J. Stat. Phys.* 3(2), 211 (1971)
46. J. S. Langer, Metastable states, *Physica* 73(1), 61 (1974)
47. K. Binder, Double-well thermodynamic potentials and spinodal curves: How real are they? *Philos. Mag. Lett.* 87(11), 799 (2007)
48. J. D. Gunton and M. C. Yalabik, Renormalization-group analysis of the mean-field theory of metastability: A spinodal fixed point, *Phys. Rev. B* 18(11), 6199 (1978)
49. W. Klein and C. Unger, Pseudospinodals, spinodals, and nucleation, *Phys. Rev. B* 28(1), 445 (1983)
50. C. Unger and W. Klein, Nucleation theory near the classical spinodal, *Phys. Rev. B* 29(5), 2698 (1984)
51. H. K. Janssen, in: Dynamical Critical Phenomena and Related topics, Lecture Notes in Physics, Vol. 104, ed. C. P. Enz, Berlin: Springer, 1979
52. H. K. Janssen, in: From Phase Transition to Chaos, eds. G. Györgyi, I. Kondor, L. Sasvári, and T. Tél, Singapore: World Scientific, 1992, and references therein
53. J. Zinn-Justin, Quantum Field Theory and Critical Phenomena, 3rd Ed., Oxford: Clarendon, 1996
54. A. N. Vasil'ev, The Field Theoretic Renormalization Group in Critical Behavior Theory and Stochastic Dynamics, London: Chapman and Hall/CRC, 2004
55. U. C. Täuber, Critical Dynamics, http://www.phys.vt.edu/∼tauber/utaeuber.html
56. R. Folk and G. Moser, Critical dynamics: A field-theoretical approach, *J. Phys. A* 39(24), R207 (2006)
57. P. C. Martin, E. D. Siggia, and H. A. Rose, Statistical dynamics of classical systems, *Phys. Rev. A* 8(1), 423 (1973)
58. R. Bausch, J. K. Janssen, and H. Wagner, Renormalized field theory of critical dynamics, *Z. Phys. B* 24(1), 113 (1976)
59. U. Deker and F. Haake, Fluctuation-dissipation theorems for classical processes, *Phys. Rev. A* 11(6), 2043 (1975)
60. C. De Dominicis and L. Peliti, Field-theory renormalization and critical dynamics above T_c: Helium, antiferromagnets, and liquid-gas systems, *Phys. Rev. B* 18(1), 353 (1978)
61. Y. Saito, Pseudocritical phenomena near the spinodal point, *Prog. Theor. Phys.* 59(2), 375 (1978)
62. D. J. Amit, Renormalization of the Potts model, *J. Phys. A* 9(9), 1441 (1976)
63. A. B. Harris, T. C. Lubensky, W. K. Holcomb, and C. Dasgupta, Renormalization-group approach to percolation problems, *Phys. Rev. Lett.* 35(6), 327 (1975)
64. S. Gong, F. Zhong, X. Huang, and S. Fan, Finite-time scaling via linear driving, *New J. Phys.* 12(4), 043036 (2010)
65. F. Zhong, Finite-time scaling and its applications to continuous phase transitions, in: Applications of Monte Carlo Method in Science and Engineering, ed. S. Mordechai, Rijeka: Intech, 2011. Available at http://www.intechopen.com/articles/show/title/finite-time-scaling-and-its-applications-to-continuous-phase-transitions
66. F. Zhong, Probing criticality with linearly varying external fields: Renormalization group theory of nonequilibrium critical dynamics under driving, *Phys. Rev. E* 73(4), 047102 (2006)
67. P. Jung, G. Gray, R. Roy, and P. Mandel, Scaling law for dynamical hysteresis, *Phys. Rev. Lett.* 65(15), 1873 (1990)
68. V. L. Ginzburg, Some remarks on phase transitions of the second kind and the microscopic theory of ferroelectric materials, *Sov. Phys. Solid State* 2, 1824 (1960)
69. D. J. Amit, The Ginzburg criterion-rationalized, *J. Phys. C: Solid State Phys.* 7, 3369 (1974)
70. K. Binder, Nucleation barriers, spinodals, and the Ginzburg criterion, *Phys. Rev. A* 29(1), 341 (1984)
71. E. Brézin, J. C. Le Guillou, and J. Zinn-Justin, in: Phase Transitions and Critical Phenomena, eds. C. Domb and M. S. Green, Vol. 6, New York: Academic, 1976
72. D. J. Amit and V. Martin-Mayer, Field Theory, the Renormalization Group, and Critical Phenomena, 3rd Ed., Singapore: World Scientific, 2005
73. K. Symanzik, Massless ϕ^4 theory in 4-ε dimensions theory in 4-ε dimensions, *Lett. Nuovo Cimento* 8(13), 771 (1973)
74. G. Parisi, Field-theoretic approach to second-order phase transitions in two- and three-dimensional systems, *J. Stat. Phys.* 23(1), 49 (1980)
75. M. C. Bergère and F. David, Nonanalyticity of the perturbative expansion for super-renormalizable massless field theories, *Ann. Phys.* 142(2), 416 (1982)
76. C. Bagnuls and C. Bervillier, Nonasymptotic critical behavior from field theory at $d = 3$: The disordered-phase case, *Phys. Rev. B* 32(11), 7209 (1985)

77. C. Bagnuls, C. Bervillier, D. I. Meiron, and B. G. Nickel, Nonasymptotic critical behavior from field theory at $d = 3$ (II): The ordered-phase case, *Phys. Rev. B* 35(7), 3585 (1987)
78. R. Schloms and V. Dohm, Minimal renormalization without ε-expansion: Critical behavior in three dimensions, *Nucl. Phys. B* 328(3), 639 (1989)
79. G. 't Hooft and H. Veltman, Regularization and renormalization of gauge fields, *Nucl. Phys. B* 44(1), 189 (1972)
80. S. Fan and F. Zhong, Evidences of the instability fixed points of first-order phase transitions, *J. Stat. Phys.* 143(6), 1136 (2011)
81. H. K. Janssen, B. Schaub, and B. Schmittmann, New universal short-time scaling behaviour of critical relaxation processes, *Z. Phys. B* 73(4), 539 (1989)
82. F. W. Wegner, Corrections to scaling laws, *Phys. Rev. B* 5(11), 4529 (1972)
83. P. G. de Gennes, Phenomenology of short-range-order effects in the isotropic phase of nematic materials, *Phys. Lett. A* 30(8), 454 (1969)
84. R. G. Priest and T. C. Lubensky, Critical properties of two tensor models with application to the percolation problem, *Phys. Rev. B* 13(9), 4159 (1976)
85. R. B. Potts and C. Domb, Some generalized order-disorder transformations, *Proc. Camb. Philos. Soc.* 48(01), 106 (1952)
86. R. K. P. Zia and D. J. Wallace, Critical behavior of the continuous n-component Potts model, *J. Phys. A* 8(9), 1495 (1975)
87. C. M. Fortuin and P. W. Kasteleyn, On the random-cluster model, *Physica* 57(4), 536 (1972)
88. S. F. Edwards and P. W. Anderson, Theory of spin glasses, *J. Phys. F* 5(5), 965 (1975)
89. A. B. Harris, T. C. Lubensky, and J.-H. Chen, Critical properties of spin-glasses, *Phys. Rev. Lett.* 36, 415 (1976)
90. G. Ódor, Universality classes in nonequilibrium lattice systems, *Rev. Mod. Phys.* 76(3), 663 (2004)
91. G. Ódor, Universality in Nonequilibrium Lattice Systems, Singapore: World Scientific, 2008
92. H. K. Janssen and U. C. Täuber, The field theory approach to percolation processes, *Ann. Phys.* 315(1), 147 (2005)
93. H. D. I. Abarbanel, J. D. Bronzan, R. L. Sugar, and A. R. White, Reggeon field theory: Formulation and use, *Phys. Rep.* 21(3), 119 (1975)
94. M. Moshe, Recent developments in Reggeon field theory, *Phys. Rep.* 37(3), 255 (1978)
95. J. L. Cardy and R. L. Sugar, Directed percolation and Reggeon field theory, *J. Phys. A* 13(12), L423 (1980)
96. G. Parisi and N. Sourlas, Critical behavior of branched polymers and the Lee–Yang edge singularity, *Phys. Rev. Lett.* 46(14), 871 (1981)
97. T. C. Lubensky and A. J. McKane, Anderson localization, branched polymers and the Yang–Lee edge singularity, *J. Phys. Lett.* 42(14), 331 (1981)
98. J. L. Cardy, Directed lattice animals and the Lee–Yang edge singularity, *J. Phys. A* 15(11), L593 (1982)
99. A. J. McKane, D. J. Wallace, and R. K. P. Zia, Models for strong interactions in 6-ϵ dimensions, *Phys. Lett. B* 65(2), 171 (1976)
100. O. F. A. Bonfim, J. E. Kirkham, and A. J. McKane, Critical exponents to order ϵ^3 for ϕ^3 models of critical phenomena in 6-ϵ dimensions, *J. Phys. Math. Gen.* 13(7), L247 (1980)
101. O. F. A. Bonfirm, J. E. Kirkham, and A. J. McKane, Critical exponents for the percolation problem and the Yang–Lee edge singularity, *J. Phys. Math. Gen.* 14(9), 2391 (1981)
102. A. J. McKane, Vacuum instability in scalar field theories, *Nucl. Phys. B* 152(1), 166 (1979)
103. J. E. Kirkham and D. J. Wallace, Comments on the field-theoretic formulation of the Yang–Lee edge singularity, *J. Phys. A* 12(2), L47 (1979)
104. A. Houghton, J. S. Reeve, and D. J. Wallace, High-order behavior in φ^3 field theories and the percolation problem, *Phys. Rev. B* 17(7), 2956 (1978)
105. D. J. Amit, D. J. Wallace, and R. K. P. Zia, Universality in the percolation problem — Anomalous dimensions of φ^4 operators, *Phys. Rev. B* 15(10), 4657 (1977)
106. D. J. Elderfield and A. J. McKane, Relevance of φ^4 operators in the Edwards–Anderson model, *Phys. Rev. B* 18(7), 3730 (1978)
107. C. N. Yang and T. D. Lee, Statistical theory of equations of state and phase transitions (I): Theory of condensation, *Phys. Rev.* 87(3), 404 (1952)
108. T. D. Lee and C. N. Yang, Statistical theory of equations of state and phase transitions (II): Lattice gas and Ising model, *Phys. Rev.* 87(3), 410 (1952)
109. P. J. Kortman and R. B. Griffiths, Density of zeros on the Lee–Yang circle for two Ising ferromagnets, *Phys. Rev. Lett.* 27(21), 1439 (1971)
110. D. A. Kurtze and M. E. Fisher, Yang–Lee edge singularities at high temperatures, *Phys. Rev. B* 20(7), 2785 (1979)
111. N. Breuer and H. K. Janssen, Equation of state and dynamical properties near the Yang–Lee edge singularity, *Z. Phys. B* 41(1), 55 (1981)
112. J. Reeve, A. J. Guttmann, and B. Keck, Critical behavior of φ^3 field theories in three dimensions, *Phys. Rev. B* 26(7), 3923 (1982)
113. See, e.g., L. H. Ryder, Quantum Field Theory, 2nd Ed., Cambridge: Cambridge University Press, 2004
114. F. Zhong, Imaginary fixed points can be physical, *Phys. Rev. E* 86(2), 022104 (2012)